# *FUS* gene is dual-coding with both proteins united in molecular hallmarks of amyotrophic lateral sclerosis

Marie A. Brunet[1, 2,*], Jean-Francois Jacques[1,2], Sonya Nassari[3], Giulia E. Tyzack[4,5], Philip McGoldrick[6], Lorne Zinman[7], Steve Jean[3], Janice Robertson[6], Rickie Patani[4,5], Xavier Roucou[1, 2,*]

[1] Department of Biochemistry, Université de Sherbrooke, Sherbrooke, Québec, Canada;

[2] PROTEO, Quebec Network for Research on Protein Function, Structure, and Engineering;

[3] Anatomy and Cell Biology Department, Université de Sherbrooke, Sherbrooke, Québec, Canada;

[4] The Francis Crick Institute, 1 Midland Road, London, UK;

[5] Department of Neuromuscular Diseases, UCL Queen Square Institute of Neurology, Queen Square, London, UK;

[6] Tanz Centre for Research in Neurodegenerative Diseases, University of Toronto, Toronto, Canada;

[7] Division of Neurology, Department of Medicine, Sunnybrook Health Sciences Centre, University of Toronto, Toronto, Canada.

[*]Corresponding authors:

Xavier Roucou, Department of Biochemistry, Université de Sherbrooke, 3201 Jean Mignault, Sherbrooke, Québec J1E 4K8, Canada, Tel. (819) 821-8000x72240; E-Mail: xavier.roucou@usherbrooke.ca

22 Marie A. Brunet, Department of Biochemistry, Université de Sherbrooke, 3201 Jean Mignault,
23 Sherbrooke, Québec J1E 4K8, Canada, Tel. (819) 821-8000x72189; E-Mail:
24 marie.brunet@usherbrooke.ca

25

26

27 **ABSTRACT:**

28 Novel functional coding sequences (altORFs) are camouflaged within annotated ones (CDS) in a
29 different reading frame. We discovered an altORF nested in the FUS CDS encoding a conserved
30 protein, altFUS. We thus demonstrate the dual-coding nature of the Amyotrophic Lateral Sclerosis
31 (ALS)-associated *FUS* gene. AltFUS is endogenously expressed in human tissues, notably in the
32 motor cortex and motor neurons of healthy controls and ALS patients. AltFUS inhibits autophagy,
33 a pathological hallmark presently and incorrectly attributed to the FUS protein. AltFUS is pivotal
34 in two other pathological hallmarks: loss of mitochondrial membrane potential and accumulation
35 of FUS/TDP-43 cytoplasmic aggregates. Suppression of altFUS expression in a *FUS*-ALS *Drosophila*
36 model protects against neurodegeneration. Thus, wild-type altFUS is essential for ALS-like
37 phenotypes arising from mutated FUS. Some mutations found in ALS patients are overlooked
38 because of their synonymous effect on the FUS protein, yet we showed they exert a deleterious
39 effect via their missense consequence on the overlapping altFUS protein. These findings suggest
40 that both proteins, FUS and altFUS, are involved in the aetiology and pathological hallmarks of
41 ALS.

42

43

44 **MAIN**

45 Amyotrophic Lateral Sclerosis (ALS) is a fatal motor neuron degenerative disease[1–3] characterized
46 by a progressive loss of motor neurons in the brain, brainstem and spinal cord[1]. Most cases are
47 sporadic (sALS), although up to 10 % are familial (fALS)[2]. The first gene associated with ALS (*SOD1*)
48 was described in 1993[4]. Since then, over 25 genes have been associated with fALS, sALS or both,
49 with the four most common being *C9ORF72*, *SOD1*, *FUS*, and *TARDBP* [2,5]. Notably, mutations in
50 *FUS* are linked to both fALS and sALS, and present some of the earliest and more rapidly
51 progressive forms of the disease[6–8]. *FUS* is also involved in other neurodegenerative diseases, such
52 as frontotemporal dementia (FUS-FTLD), all characterized by FUS cytoplasmic inclusions[9].

53 FUS is a nuclear RNA-binding protein, with a C-terminal nuclear localization signal (NLS)[9,10]. The
54 protein is involved in RNA processing, DNA repair and cellular proliferation, although its functions
55 are not precisely elucidated[9]. Most of the mutations associated with neurodegenerative diseases
56 alter FUS NLS[11–13]. More recently, mutations in *FUS* 3'UTR were described in ALS patients and
57 linked to an increased level of *FUS* mRNA and protein[14–16]. Surprisingly, over-expression of wild-
58 type FUS provokes an aggressive ALS phenotype in mice and fruit flies, in accordance with findings
59 in yeast and mammalian cells[17–21]. The mechanism of the wild-type or ALS-linked mutated FUS
60 toxicity remains unclear[3,9,22].

61 With currently non-annotated proteins being increasingly reported[23–26], we hypothesized that the
62 toxicity resulting from wild-type FUS over-expression may come from another, unseen, actor[26].
63 These novel proteins are coded by alternative open reading frames (altORFs) that are located
64 within "non-coding" RNAs (ncRNA), within the 5' or 3' "untranslated" regions (UTR) of mRNAs, or
65 overlapping a known coding sequence (CDS) within a different frame of an mRNA[25–27].
66 Serendipitous discoveries and ribosome profiling have recently highlighted the distribution of

67 altORFs throughout the human genome, and the consequences of their absence from current
68 databases[26]. For example, mass spectrometry-based proteomics has become the gold standard
69 for protein identification and has been extensively used in ALS studies[28,29]. However, if a protein
70 is not annotated, it is not included in the protein database (e.g. UniProtKB), and thus cannot be
71 detected by mass spectrometry. An estimated 50 % of mass spectra from a proteomics
72 experiment are unmatched at the end of the analysis[26,30].

73 Genome annotations must avoid spurious ORF annotations. Thus unless functional
74 characterization has been published, they rely upon 2 arbitrary criteria: a minimum length of 100
75 codons and a single ORF per transcript. Several groups developed tools to challenge such criteria,
76 such as the sORFs repository[31] and the OpenProt database[27], which offer a data-driven broader
77 view of eukaryotic proteomes. The OpenProt database is based on a polycistronic model of ORF
78 annotation[27] and reports any ORF longer than 30 codons within any frame of an mRNA or ncRNA.
79 It contains currently annotated proteins (RefProts), novel Isoforms, and novel alternative proteins
80 (altProts). Here, we used the OpenProt database (www.openprot.org) to ask whether *FUS* may
81 encode additional proteins that could explain the toxicity of the wild-type protein over-
82 expression, and bring novel insights concerning *FUS*-linked ALS pathogenicity[26,27].

83

84

85 **ALTFUS IS A NOVEL 170 AMINO ACID PROTEIN, ENDOGENOUSLY EXPRESSED IN CELL LINES AND TISSUES**

86 We began by querying OpenProt[27] predictions for *FUS* canonical mRNA (*ENST00000254108* or
87 *NM_004960*), which led to 8 predicted altORFs, either overlapping the coding sequence (CDS) or
88 within the 3'UTR (**Extended Data Table 1**). Amongst these, IP_243680 or altFUS, a 170 codon
89 altORF, presents convincing experimental evidence of expression (OpenProt v1.3). AltFUS
90 overlaps the FUS CDS in an open reading frame shifted by one nucleotide (**Fig. 1a**, **Extended Data**
91 **Fig. 1a**). *FUS* is a complex gene with 13 annotated transcripts resulting from alternative splicing.
92 Based on the GTEx expression data in brain tissues and nerves, five transcripts are more abundant
93 and represent 85 % of all transcripts (**Extended Data Fig. 1b**). Three of them (*FUS-206*, *FUS-211*,
94 *FUS-203*) are non-coding according to Ensembl, while only two (*FUS-211*, *FUS-203*) are non-coding
95 according to OpenProt (**Fig. 1b**). Ensembl[32] annotates two transcripts as coding (*FUS-201* and *FUS-*
96 *202*), either for the 526 amino acid FUS protein or its 525 amino acid isoform. From OpenProt
97 prediction, these two transcripts also encode altFUS (IP_243680), or its 169 amino acid isoform
98 (IP_243691) respectively. Moreover, the second most abundant transcript in brain tissues and
99 nerves (*FUS-206*), representing about 20 % of all transcripts, is non-coding according to Ensembl,
100 but OpenProt predicts it contains the altFUS CDS (**Fig. 1b**, **Extended Data Fig. 1c**). Thus, of the five
101 most abundant transcripts in brain tissues and nerves, two code for both FUS and altFUS proteins,
102 one codes for altFUS alone, and the remaining two are non-coding.

103 Published RIBO-seq data in Human, retrieved from the Gwips portal[33], revealed an accumulation
104 of initiating ribosomes around the altFUS initiating methionine, in association with an increase in
105 the density of elongating ribosomes over altFUS CDS (**Fig. 1c**). These results suggest that altFUS is
106 translated. Similar results were observed in Mouse (**Extended Data Fig. 1d**). Additionally, we
107 retrieved nucleotide conservation scores (PhyloP) for *FUS* transcripts over 100 vertebrates. PhyloP
108 scores range from -10 (highly variable) to 10 (highly conserved). PhyloP scores over the FUS CDS

109 are under a constraint at the altFUS CDS locus (average score of 2.6 instead of 4 elsewhere on the
110 FUS CDS), which is consistent with a selection pressure across 2 overlapping frames (**Extended**
111 **Data Fig. 1e**)[34]. We then retrieved altFUS protein sequences over 84 species and observed a strong
112 protein conservation across mammals, and primates notably (75 to 99.4 % of sequence identity -
113 **Extended Data Table 2**, **Extended Data Fig. 1f and Extended Data Alignment File**). Thus, AltFUS
114 is well conserved, with domains showing little to no sequence variations (**Fig. 1d**).

115 Based on the OpenProt database, AltFUS was identified in multiple proteomics datasets, with up
116 to 7 confident unique peptides, representing a 41 % sequence coverage (**Fig. 1e, Extended Data**
117 **Table 1**). To validate altFUS protein expression, we developed a custom antibody targeting two
118 unique altFUS peptides (**Extended Data Fig. 2a**) and tested it using three constructs: FUS, altFUS
119 and FUS$^{(\emptyset)}$. The latter is a monocistronic *FUS* version, where all altFUS methionines are mutated
120 for threonines in a manner synonymous for FUS (**Extended Data Fig. 2b-d**). Thus, the FUS protein
121 sequence is unchanged, but the altFUS sequence does not contain any methionines. Transfection
122 of HEK293 cells revealed expression of both proteins, FUS and altFUS, from the FUS nucleotide
123 sequence (**Fig. 1f**). As expected, altFUS expression was lost with the monocistronic FUS$^{(\emptyset)}$
124 construct. HEK293 cells transfected with a siRNA targeting *FUS* mRNA showed a significant
125 knockdown of both proteins, FUS and altFUS; whereas altFUS endogenous expression was visible
126 in scrambled control siRNA and mock transfected cells (**Fig. 1g**). These results validate the
127 specificity of the custom antibody and demonstrate altFUS endogenous expression in HEK293
128 cultured cells.

129 AltFUS endogenous expression was visible in control human tissues, HEK293 and HeLa cell lines
130 (**Fig. 1h**). Since FUS gene is associated with ALS, which predominantly affects the motor cortex in
131 addition to the ventral spinal cord, we retrieved motor cortex lysates from 3 ALS patients with a
132 C9orf72 mutation (most common) and 3 sporadic ALS patients. AltFUS endogenous expression

133 was detected in all cases (**Fig. 1i**). Furthermore, as ALS is a motor neuron disease, we derived
134 functional ventral spinal motor neurons from induced pluripotent stem cells (iPSCs)[35,36] from
135 healthy controls and ALS patients carrying valosin-containing protein mutations (3 lines per
136 group). AltFUS endogenous expression was detected in all samples (**Fig. 1j**). We noticed that brain
137 (**Fig. 1h**) and motor cortex lysates (**Fig. 1i**), as well as iPSCs-derived motor neurons (**Fig. 1j**), from
138 healthy controls and ALS patients, presented a higher band detected with the custom altFUS
139 antibody. This band is not present in cultured cell lines or other tissues. It could come from a non-
140 specific signal or a post-translational modification on altFUS that is specific to the motor cortex
141 and spinal cord motor neurons (**Fig. 1h-j**). We could also observe a lower band in the line 2 of
142 controls motor neurons, which may correspond to a degradation product or an initiation at a
143 downstream methionine in altFUS sequence. This band has never been observed in other samples
144 so far. We demonstrate that the *FUS* gene encodes two proteins, FUS and altFUS, both
145 endogenously expressed in the motor cortex and spinal cord motor neurons, to the two
146 archetypal regions predominantly affected in ALS.

147 **ALTFUS IS A MITOCHONDRIAL PROTEIN, INVOLVED IN ALS-ASSOCIATED LOSS OF MITOCHONDRIAL MEMBRANE**
148 **POTENTIAL**

149 FLAG-tagged altFUS (altFUS-FLAG) displayed a strong co-localization with a common mitochondrial
150 marker, TOMM20 (**Fig. 2a**). Additionally, mitochondrial extracts showed an enrichment in altFUS-
151 FLAG (**Fig. 2b**). Cellular fractionation of cells over-expressing untagged altFUS further validated
152 altFUS mitochondrial localization (**Fig. 2c**). The endogenous altFUS protein was found in the
153 mitochondrial fraction, although it displayed a weak cytoplasmic signal as well (**Fig. 2d**), consistent
154 with the immunofluorescence data (**Fig. 2a**). Furthermore, cells over-expressing altFUS showed
155 an altered mitochondrial network, with a significant increase in fragmented mitochondria

156 (globular) compared to mock cells that displayed more tubular structures (**Fig. 2e, f**, **Extended**
157 **Data Fig. 3a**).

158 Mitochondrial fragmentation is observed in *FUS*-linked ALS models[37–39], and here we reproduced
159 a similar effect when over-expressing altFUS alone. Thus, we wondered whether altFUS played a
160 role in other mitochondrial dysfunctions observed in ALS. To this end, we reproduced an ALS-
161 linked FUS mutant: FUS-R495x[38,39]. This mutant leads to a premature stop codon before FUS NLS
162 and is linked to severe fALS and sALS cases[9]. In this construct, altFUS is still present and not
163 affected by the mutation. Similarly to FUS$^{(\emptyset)}$, we also generated the monocistronic construct
164 FUS$^{(\emptyset)}$-R495x, which contains synonymous mutations for FUS-R495x (**Extended Data Fig. 3b)**, but
165 prevents altFUS expression (**Fig. 1f**). V5-FUS$^{(\emptyset\text{-FLAG})}$ and V5-FUS$^{(\emptyset\text{-FLAG})}$-R495x did not express altFUS,
166 but only the FUS protein, wild-type or ALS-linked mutant R495x respectively (**Extended Data Fig.**
167 **3c**). We first investigated the effect of altFUS on the mitochondrial membrane potential using the
168 potential sensitive dye TMRE (**Fig. 2g, h, Extended Data Fig. 3d**). As previously described[38], over-
169 expression of bicistronic FUS or FUS-R495x led to a decrease in mitochondrial membrane
170 potential. The mitochondrial membrane potential remained normal when over-expressing
171 monocistronic FUS$^{(\emptyset)}$ or FUS$^{(\emptyset)}$-R495x, underlining the role of altFUS. However, over-expression of
172 altFUS alone did not alter the mitochondrial membrane potential, which suggests both proteins
173 cooperate for this ALS pathological hallmark.

174 To further evaluate the possible implication of altFUS in ALS, we investigated its protein
175 interactors. Using stimulated emission depletion microscopy (STED), we observed that altFUS
176 localized in puncta following a cristae-like pattern inside the mitochondria, delimited using an
177 outer-membrane mitochondrial marker, TOMM20 (**Fig. 2i, j**). We then used size-exclusion
178 chromatography on mitochondrial extracts to isolate altFUS-FLAG macromolecular complexes (**Fig.**
179 **2k**). Following a FLAG affinity purification and mass spectrometry analysis, we identified 16

180 interacting proteins (**Fig. 2l**, **Extended Data Table 3**). A gene enrichment analysis to the Human
181 mitochondrial proteome identified three significantly enriched biological processes: autophagy-
182 related pathways, mitochondrial metabolism and cellular response to stress (**Fig. 2m**). Disruptions
183 within these are pathological hallmarks of ALS[3,21,39,40].

184 **ALTFUS INHIBITS AUTOPHAGY AND DRIVES THE ACCUMULATION OF FUS- AND TDP43-POSITIVE CYTOPLASMIC**
185 **AGGREGATES**

186 Following on these results, we hypothesized that the inhibition of autophagy observed with ALS-
187 linked FUS mutants may instead be attributed to altFUS. We used the mCherry-GFP-LC3 reporter
188 to track the autophagic flux by confocal microscopy (**Extended Data Fig. 4a**). Under basal
189 conditions, cells displayed red and yellow foci as expected (**Fig. 3a**). An accumulation of yellow
190 foci was observed when cells were treated with bafilomycin, an inhibitor of autophagy. Similarly,
191 cells over-expressing altFUS displayed a significant accumulation of yellow foci (**Fig. 3a**). Our
192 results were consistent with previously published data[11] as cells transfected with FUS or FUS-
193 R495x displayed a decreased autophagic flux (**Fig. 3a, Extended Data Fig. 4b**). This accumulation
194 of yellow foci was absent in cells that express monocistronic FUS constructs, thus lacking altFUS
195 expression ($FUS^{(\emptyset)}$ or $FUS^{(\emptyset)}$-R495x). We used bafilomycin followed by LC3 probing to further
196 validate the impact of altFUS on autophagy (**Fig. 3b, Extended Data Fig. 4c**). Similarly, an inhibition
197 of autophagy was observed only in cells over-expressing altFUS. Furthermore, in cells over-
198 expressing monocistronic $FUS^{(\emptyset)}$-R495x, the inhibition of autophagy could be restored by co-
199 transfecting altFUS (**Fig. 3b**). These results establish altFUS, rather than FUS, as the protein
200 responsible of the inhibition of autophagy.

201 Furthermore, altFUS interactome analysis suggested a role in the cellular stress response, which
202 is known to be altered in ALS with a TDP-43 cytoplasmic accumulation in 98 % of patients[41,42]. In

203 *FUS*-linked ALS and some sALS cases, FUS cytoplasmic aggregates or mislocalization are also
204 observed[43–45]. We demonstrated that cells over-expressing FUS-R495x displayed cytoplasmic
205 aggregates that were positive for both FUS-R495x and TDP-43 (**Fig. 3c**). In cells over-expressing
206 the monocistronic FUS$^{(\emptyset)}$-R495x construct, thus lacking altFUS expression, FUS-R495x displayed a
207 more diffuse cytoplasmic localization, and TDP-43 remained in the nucleus (**Fig. 3c**). FUS
208 cytoplasmic aggregates were significantly more numerous and larger when altFUS was co-
209 expressed (**Fig. 3d, e**). Accumulation of FUS-R495x and TDP-43 in cytoplasmic aggregates could
210 be reconstituted by co-transfecting altFUS and the monocistronic FUS$^{(\emptyset)}$-R495x construct (**Fig. 3c**).
211 These observations were repeated across all 7 ALS-linked FUS mutations tested (**Extended Data**
212 **Fig. 4d-f**). The cytoplasmic aggregates were also TIAR-positive as observed with ALS-linked FUS
213 mutants in previous work[41] (**Extended Data Fig. 5a, b-d**). These results suggest a strong interplay
214 between FUS and altFUS in ALS and that altFUS plays a pivotal role in the assembly of cytoplasmic
215 FUS/TDP-43 aggregates.

216 **ALTFUS PROTECTS AGAINST NEURODEGENERATION IN FUS-ASSOCIATED DROSOPHILA MODELS**

217 In order to investigate the role of altFUS in ALS, we generated *Drosophila* models expressing either
218 the bicistronic, FUS and FUS-R495x constructs, or the monocistronic, FUS$^{(\emptyset)}$ and FUS$^{(\emptyset)}$-R495x,
219 constructs. We used the Elav-GeneSwitch-GAL4 Driver strain, as previously described[46], as it
220 allows for an inducible over-expression in motor neurons and avoids lethality at the larval stage
221 from FUS over-expression in the central nervous system[46,47]. First, we generated flies containing
222 the sequences for UASt-altFUS, UASt-FUS, UASt-FUS$^{(\emptyset)}$, UASt-FUS-R495x or UASt-FUS$^{(\emptyset)}$-R495x.
223 These flies were then crossed with the Elav-GeneSwitch-GAL4 driver strain (**Fig. 4a**). UASt-
224 mCherry flies were used as controls. Selected F1 individuals were then divided into 2 groups with
225 equal proportions of males/females. The first group received standard food, while the other
226 received RU-486 treated food. The treatment induces a conformational change in the Elav-

227 GeneSwitch driver, which allows activation of the UAS promoter and thus expression of the target
228 protein. We retrieved flies at selected time points to validate protein expression in the RU-486
229 treated population through time, while the controls showed no expression (**Fig. 4b**).

230 The motor neuron degeneration linked to ALS provokes a progressive locomotion loss measurable
231 with a well-described climbing assay[48]. The control populations did not show any significant
232 locomotion loss at day 1, 10 nor 20 (**Fig. 4c-e**); similarly to the RU-486 treated control group
233 (mCherry transgenic flies – **Fig. 4c**). AltFUS flies did not show any significant locomotion loss
234 through time (**Fig. 4c**). This result is consistent with the *in cellulo* data showing altFUS alone is not
235 sufficient to provoke pathological hallmarks. As previously shown with this model[19], the
236 bicistronic FUS flies, which express both FUS and altFUS proteins, displayed a significant
237 locomotion loss (**Fig. 4d**). Bicistronic ALS-linked FUS-R495x flies showed an even greater motor
238 neuron degeneration through time compared to FUS (**Fig. 4e**). Monocistronic $FUS^{(\emptyset)}$ (**Fig. 4d**) and
239 $FUS^{(\emptyset)}$-R495x (**Fig. 4e**) flies, which do not express altFUS, displayed both a delay in the onset of
240 motor neuron degeneration and a reduced drop in climbing success at 20 days post-induction
241 (40% vs. 60% for $FUS^{(\emptyset)}$, 30% vs. 70% for $FUS^{(\emptyset)}$-R495x). These results in *Drosophila* confirm a role
242 for altFUS in ALS-like neurodegeneration *in vivo*, are consistent with our *in cellulo* observations
243 and highlight the pathological cooperation between FUS and altFUS.

244 **ALS-LINKED MUTATIONS, SYNONYMOUS FOR FUS, ALTER ALTFUS AND LEAD TO TDP-43 CYTOPLASMIC**
245 **AGGREGATES**

246 As of today, over 50 mutations in the *FUS* gene have been associated with ALS[9]. However, most
247 of these locate at the carboxyl end of the protein and as such have no effect on altFUS. We
248 wondered whether mutations altering altFUS may have been overlooked as non-consequential in
249 the FUS reading frame. We retrieved FUS synonymous mutations found in ALS patients, with an

250 allelic frequency below 0.01 %, from previous studies and the ALS Variant Server
251 (http://als.umassmed.edu/ - **Extended Data Table 4**). The retrieved mutations clustered on the
252 altFUS locus, with 60 % of FUS synonymous mutations found in sALS patients and 50 % of FUS
253 synonymous mutations found in fALS patients, which is significantly higher than expected by
254 chance (34 %) (**Extended Data Table 4**). We selected 4 mutations for further analysis based on
255 the residue conservation: altFUS-P31L, altFUS-A38V, altFUS-A46V and altFUS-R64P. We generated
256 them in GFP-FUS constructs: GFP-FUS$^{(P31L\text{-}FLAG)}$-S44=; GFP-FUS$^{(A38V\text{-}FLAG)}$-G51=; GFP-FUS$^{(A46V\text{-}FLAG)}$-G59=
257 and GFP-FUS$^{(R64P\text{-}FLAG)}$-S77= (**Fig. 5a**). All altFUS mutants still localized to the mitochondria (**Fig. 5b**).
258 To investigate whether these mutations may provoke an ALS phenotype, we quantified the
259 number of cells presenting TDP-43 aggregates. All 4 altFUS mutants showed a 1.8 to 2.4 fold
260 increase compared to wild-type altFUS (**Fig 5c, d**). This result indicates that altFUS mutations
261 potentiate TDP-43 cytoplasmic aggregation, a pathological hallmark in 98 % of ALS cases. Hence,
262 some *FUS* mutations, synonymous for the FUS protein, exert a deleterious effect through their
263 missense consequence on the altFUS protein.

## 264 CONCLUSIONS: FUS AND ALTFUS, ENCODED BY THE SAME GENE, COOPERATE IN ALS-LINKED TOXIC
## 265 DYSFUNCTIONS

266 Despite considerable advances in the field, current genome annotations still uphold arbitrary
267 assumptions, such as the monocistronic nature of eukaryotic genes[26]. Here, we demonstrate *FUS*
268 is a bicistronic gene. We discovered FUS CDS contains a second protein-coding sequence in a
269 shifted frame overlapping its prion-like intrinsically disordered domain, regions known to host
270 dual-coding events[49,50]. This novel protein, named altFUS, is not an isoform but an entirely new
271 sequence of 170 amino acids. AltFUS is endogenously expressed in human tissues and cultured
272 cell lines, as demonstrated by ribosome profiling, mass spectrometry and with a custom antibody.
273 AltFUS is notably expressed in the motor cortex and iPSCs-derived motor neurons of healthy

274 controls and ALS patients. Because altFUS is embedded within the FUS CDS, this discovery is of
275 crucial importance to the field. Indeed, over-expression studies on *FUS* actually implicate two
276 proteins: FUS and altFUS. Similarly FUS knockdown or knockout studies actually inhibit expression
277 of both proteins[51]. Moreover, previous work has shown that gene editing techniques targeting a
278 specific CDS do not necessarily result in knockout of the gene in case of dual-coding gene[52]. Our
279 discovery thus suggests that *FUS* edited cells or models, notably targeting its last exons[53–55], might
280 only impair FUS protein expression but not altFUS, thus not resulting in a true *FUS* knockout. Our
281 work provides an unprecedented and much needed reconsidered view of *FUS* coding potential to
282 better understand its role, notably in the context of ALS and other neurodegenerative diseases.

283 Following the discovery of altFUS, we developed tools in order to differentiate the specific roles
284 and phenotypes of FUS and altFUS. Our study demonstrates that altFUS is necessary for three ALS
285 pathological hallmarks: mitochondrial fragmentation and loss of membrane potential, inhibition
286 of autophagy, and cytoplasmic aggregation of FUS/TDP-43. The inhibition of autophagy was
287 observed when over-expressing altFUS alone, absent when over-expressing FUS alone (wild-type
288 or ALS-associated R495x mutant) and reconstituted when co-expressing FUS and altFUS. This
289 demonstrates that the inhibition of autophagy, previously described in FUS-linked ALS[11,21], has
290 been incorrectly associated to the FUS protein. AltFUS inhibits autophagy. AltFUS is necessary but
291 not sufficient for the mitochondrial membrane potential loss and cytoplasmic aggregation of FUS
292 and TDP-43. Although TDP-43 aggregates are not commonly seen with FUS mutations[45], this study
293 lends support for altFUS conspiring with FUS and TDP-43 to lead to this molecular hallmark of ALS.
294 Our data suggests the stoichiometry between FUS and altFUS may be important for the
295 development of cytoplasmic aggregates in ALS. Both proteins are required to observe the
296 phenotype, highlighting a functional alliance between FUS and altFUS. This pathological synergy
297 was also observed in the *Drosophila* model.

298 The physiological function of altFUS is still unclear, although our work provides evidence for its
299 role in mitochondrial dynamics and the cellular response to stress. One mechanism put forward
300 in ALS is that the disease originates from a sub-optimal resolution of cellular stresses, which can
301 come from environmental sources or mutated proteins[40,56]. We have shown that altFUS, not FUS,
302 inhibits autophagy, most likely via its interaction partners (**Extended Data Table 3**). Since an
303 inhibition of autophagy inhibits the dissociation of stress granules[40], we suggest altFUS
304 potentiates stress granule accumulation under stress conditions, and that FUS phase separation
305 properties then lead to the formation of solid and toxic aggregates[57]. Further work is needed to
306 fully understand the role of altFUS in physiological and pathological conditions, yet our study
307 shows this novel protein plays a crucial role in *FUS*-linked gain-of-toxic dysfunctions observed in
308 ALS. Hence, *FUS* should be recognized and annotated as a polycistronic gene.

309 Recent studies have addressed the toxicity resulting from over-expression of wild-type FUS.
310 Bogaert and colleagues used FUS domain truncation mutants to investigate wild-type FUS toxicity.
311 A FUS mutant lacking its N-terminal intrinsically disordered domain, thus lacking altFUS, displayed
312 reduced toxicity. This study corroborates our findings that the absence of altFUS reduces the
313 toxicity. Furthermore, Bogaert and colleagues concluded that FUS N-terminal synergizes with the
314 C-terminal domain to mediate toxicity in *Drosophila*[47]. Here, we showed that altFUS synergizes
315 with FUS to mediate ALS pathological features in cultured cells and toxicity in *Drosophila*. Despite
316 different laboratories and different techniques, our data are in agreement with theirs. Yet, we
317 point to an alternative (not necessarily mutually exclusive) explanation whereby altFUS, not the
318 FUS N-terminal domain, synergizes for toxicity. Additionally, this discussion shows that not being
319 aware of overlapping CDSs, especially in deletion studies, precludes alternative interpretations.

320 Current genome annotations guide the interpretation of data and the design of studies, however
321 they also affect the way we screen for pathological mutations[26]. Most of the ALS-linked *FUS*

322 mutations affect the carboxyl end of the protein, as shown with the example used in this study,
323 the R495x mutation[13]. These mutations do not alter the altFUS protein, which is embedded at the
324 beginning of the FUS CDS and span on exons 3 to 6. How could altFUS be important for the disease
325 if most pathological mutations do not alter it? To answer this question, one needs to grasp how
326 much genome annotations shape today's research. For example, when screening for pathological
327 mutations, those that are synonymous for FUS are discarded early in analyses as insignificant[58].
328 Yet, a synonymous mutation for FUS may not be for altFUS. Our work shows that FUS synonymous
329 mutations found in patients cluster on altFUS genomic locus. We tested 4 of these mutations,
330 synonymous for the FUS protein and missense for the altFUS protein, and we found that each of
331 them potentiated TDP-43 cytoplasmic aggregation, a pathological hallmark of ALS[42]. Thus, *FUS* is
332 a double-edge genetic source of ALS, with both of its proteins involved in the aetiology of the
333 disease.

334 This work demonstrates the importance of genome annotation in our quest to better understand
335 physiological and pathological mechanisms and serves as a proof-of-concept to acknowledge the
336 polycistronic coding potential of eukaryotic genes[26]. For example, taking the 16 genes associated
337 with ALS as reviewed in Taylor and colleagues, 56 % (9) of them display at least one currently non-
338 annotated protein that has been detected by mass spectrometry (44 %) or ribosome profiling (31
339 %) according to the OpenProt database (**Extended Data Table 5**)[3,27]. Several studies have
340 highlighted the biological function of currently non-annotated proteins, and intriguingly a
341 functional cooperation between proteins from the same gene is often observed[23,26,52,59–61].
342 Furthermore, a quantitative proteomic study looked at the relative abundance of two proteins
343 from the bicistronic *MIEF1* gene, MiD51 and altMiD51. The major product of *MIEF1* gene is the
344 novel protein, altMiD51 (now annotated as L0R8F8 in UniProtKB), as shown in cell lines and

345 healthy colon tissue[52]. AltFUS is the first example of an alternative protein linked to a pathology

346 but is unlikely to be the only one.

347

348 **METHODS**

349 **FUS constructs**

350 FUS and altFUS sequences were obtained from Bio Basic Gene Synthesis service. All FUS constructs
351 were subcloned into pcDNA3.1- (Invitrogen) using Gibson assembly (New England Biolabs,
352 E26115). FUS and altFUS wild-type sequences correspond to that of the Human FUS canonical
353 transcript (*ENST00000254108* or *NM_004960*). FUS and altFUS proteins were tagged with V5
354 (GKPIPNPLLGLDST) and 2 FLAG (DYKDDDDKDYKDDDDK) respectively. FUS was tagged on the N-
355 terminal, altFUS was tagged on the C-terminal. For immunofluorescence assays, N-terminal GFP-
356 tagged FUS was also cloned into pcDNA3.1- by Gibson assembly. The necessary gBlocks were
357 purchased from IDT. The monocistronic constructs $FUS^{(\emptyset)}$ and $FUS^{(\emptyset)}$-R495x were generated by
358 mutating all altFUS methionines (ATG) to threonines (ACG). These mutations are synonymous in
359 the FUS CDS (TAT > TAC, both coding for tyrosine). The altFUS mutated sequence was obtained
360 from Bio Basic Gene Synthesis service, and then subcloned in FUS sequences in pcDNA3.1- using
361 Gibson assembly. The bicistronic constructs are named as follows throughout the article: FUS,
362 FUS-R495x, or $FUS^{(FLAG)}$ and $FUS^{(FLAG)}$-R495x when altFUS is FLAG-tagged in the +2 reading frame. The
363 monocistronic constructs are named as follows throughout the article: $FUS^{(\emptyset)}$ or $FUS^{(\emptyset)}$-R495x to
364 indicate altFUS absence.

365 **Cell culture, transfections, western blots and immunofluorescence**

366 HEK293 and HeLa cells cultures tested negative for mycoplasma contamination (ATCC 30–1012K).
367 Transfections, immunofluorescence, confocal analyses and western blots were carried out as
368 previously described[60]. For FUS knock-down, 150 000 HEK293 cells in a 6-well plate were
369 transfected with 25 nM FUS SMARTpool: siGENOME siRNA (Dharmacon, Canada, L-009497-00-
370 0005) or ON-TARGET plus Nontargeting pool siRNAs (Dharmacon, D-001810-10-05) with
371 DharmaFECT one transfection reagent (Dharmacon, T-2001–02) according to the manufacturer's

372 protocol. Cell media was changed every 24 hrs and cells were processed 72 hrs after transfection.
373 For immunofluorescence, primary antibodies were diluted as follows: anti-Flag (Sigma, F1804) 1/
374 1000, anti-TOMM20 (Abcam, ab186734) 1/500, anti-V5 (Cell Signalling Technologies, #13202)
375 1/1000, anti-TDP-43 (ProteinTech, 10782-2-AP) 1/500, and anti-TIAR (Cell Signalling Technologies,
376 #8611) 1/1600. For western blots, primary antibodies were diluted as follows: anti-Flag (Sigma,
377 F1804) 1/8000, anti-V5 (Sigma, V8012) 1/8000, anti-actin (Sigma, A5441) 1/40000, anti-FUS
378 (Abcam, ab84078) 1/500, anti-altFUS (Abcam, custom antibody) 1/3000, anti-LC3 (Cell Signalling
379 Technologies, #2775) 1/1000, anti-Hsp70 (Thermo Fisher Scientific, MA3-028) 1/1000, anti-
380 Tubulin (Thermo Fisher Scientific, a11126) 1/2000 and anti-VDAC (Abcam, ab15895) 1/10000. The
381 altFUS antibody was generated by injection two rabbits, each with 2 unique altFUS peptide. The
382 purified antibody from rabbit 2 was used in this study at a 1/2000 dilution. Mitochondrial
383 morphology was evaluated using the microP tool[62]. A minimum of 100 cells per replicate were
384 counted across 3 independent experiments (n = 3, i.e. minimum 300 cells for each experimental
385 condition). Colocalization analyses were performed using the JACoP plugin (Just Another
386 Colocalization Plugin) implemented in Image J software, as previously described[23]. When
387 specified, images obtained by confocal microscopy on the Leica TCS SP8 STED 3X were
388 deconvolved using the Huygens software (Scientific Volume Imaging B.V., Hilversum,
389 Netherlands). The software uses a signal reassignment algorithm for deconvolution, identical
390 deconvolution parameters were applied to all images. The default parameters were used,
391 including the Classic Maximum Likelihood Estimation (CMLE) algorithm, signal to noise ratio, and
392 background estimation radius. The maximum iteration number was set at 30. Human tissue
393 lysates for altFUS endogenous expression were purchased from Zyagen Laboratories (San Diego,
394 California, USA).

395 **RIBO-seq data and conservation analyses**

396 Global aggregate reads for initiating ribosomes and elongating ribosomes footprints across all
397 available studies were downloaded from the Gwips portal (https://gwips.ucc.ie/), for *Homo*
398 *sapiens* and for *Mus musculus*. For altFUS protein conservation analysis, all FUS mRNAs with at
399 least EST evidence were retrieved across all available species from NCBI RefSeq. We performed
400 an *in silico* 3-frame translation and retrieved the best matching protein sequence per species that
401 displayed a minimum of 20 % sequence identity with the Human altFUS sequence over 25 % of
402 Human altFUS length. AltFUS homologous sequences were found in 83 species, and we manually
403 added that of *Drosophila melanogaster* that displayed a 37.5 % sequence identity over 19 % of
404 the Human altFUS length. All retrieved altFUS sequences were then aligned using Clustalω with
405 default parameters.

406 **Human induced pluripotent stem cell differentiation into motor neurons**

407 Directed differentiation to human iPSC-motor neurons was performed as previously reported[35].
408 Briefly, iPSCs were maintained on Geltrex (Life Technologies) with Essential 8 Medium media (Life
409 Technologies), and passaged using EDTA (Life Technologies, 0.5mM). All cell cultures were
410 maintained at 37°C and 5% carbon dioxide. For motor neuron differentiation, iPSCs were
411 differentiated to neuroepithelium by plating to 100% confluency in chemically defined medium
412 consisting of DMEM/F12 Glutamax, Neurobasal, L-Glutamine, N2 supplement, non-essential
413 amino acids, B27 supplement, β-mercaptoethanol (Life Technologies) and insulin (Sigma).
414 Treatment with the following small molecules from day 0-7: 1µM Dorsomorphin (Millipore), 2µM
415 SB431542 (Tocris Bioscience), and 3.3µM CHIR99021 (Miltenyi Biotec). At day 8, cells patterned
416 for 7 days with 0.5µM retinoic acid and 1µM Purmorphamine. At day 14 spinal cord motor neuron
417 precursors were treated with 0.1µM Purmorphamine for a further 4 days before being terminally
418 differentiated for >10 days in 0.1 µM Compound E (Enzo Life Sciences) to promote cell cycle exit.

419 Throughout the neural conversion and patterning phase (D0-18) the neuroepithelial layer was
420 enzymatically dissociated twice (at D4-5 and D10-12) using dispase (GIBCO, 1 mg ml-1).

421 **Preparation of tissue lysates of the motor cortex of ALS patients**

422 Approximately 100mg of motor cortex from 4 sporadic ALS and 4 C9orf72-ALS cases was lysed in
423 10x RIPA (50mM Tris HCl pH7.8, 150mM NaCl, 0.5% sodium deoxycholate, 1% NP40;
424 supplemented with protease inhibitors and EDTA) volume using TissueLyzer equipment (Qiagen).
425 Lysates were incubated on ice 20 minutes followed by centrifugation at 20,000xg for 20 minutes
426 at 4°C. Supernatant was taken as 'RIPA fraction' and pellets resuspended in RIPA and SDS (final
427 concentration of 2%). 3 sporadic ALS and 3 C9orf72-ALS samples were subsequently used as they
428 were sufficiently concentrated to load 100 ug of proteins onto SDS-page gels.

429 **Mitochondrial extracts and cellular fractionation**

430 Mitochondrial extracts were prepared as previously described[52]. Briefly, HEK293 cells grown up
431 to 80 % confluence, were rinsed twice with PBS and gathered using a cell scraper. Cells were
432 pelleted by centrifugation at 500 x g for 10 mins at 4 °C. Supernatant was discarded and cells
433 suspended in mitochondrial buffer (210 mM mannitol, 70 mM sucrose, 1 mM EDTA, 10 mM
434 HEPES-NaOH, pH 7.5, 0.5 mM PMSF and EDTA-free protease inhibitor (Thermo Fisher Scientific)).
435 Cells were disrupted by 15 consecutive passages through a 25G1 0.5 x 25 needle syringe on ice,
436 followed by a 3 min centrifugation at 2 000 x g at 4 °C. Supernatant was collected and the pellet
437 suspended in mitochondrial buffer. The cell disruption was repeated four times and all retrieved
438 supernatants containing mitochondria were again passed through syringe needle in mitochondrial
439 buffer and cleared by centrifugation for 3 mins at 2000 × g at 4 °C. Supernatants were pooled and
440 centrifuged for 10 mins at 13 000 x g at 4 °C to pellet mitochondria. The pellet was suspended in
441 200 µL of mitochondrial buffer until further processing. Cellular fractionation was performed
442 using the Cell Fractionation Kit (#9038S, Cell Signaling Technology). Briefly, HEK293 cells were

443 grown up to 80 % confluence, washed twice with PBS and gathered using a cell scraper. Cells were
444 spun at 350 x g for 5 mins at 4 °C and 2.5 x $10^6$ cells were suspended in 500 µL of ice-cold PBS. An
445 aliquot of 100 µL was spun at 350 x g for 5 mins at 4 °C and resuspended in SDS buffer (4 % SDS,
446 Tris-HCl 100 mM pH 7.6) and kept as WCL (Whole Cell Lysate). The rest of the collected cells
447 (remaining 400 µL) were spun at 500 x g for 5 mins at 4 °C. Supernatant was discarded and pellet
448 resuspended in 500 µL of CIB (Cytoplasmic Isolation Buffer) from the kit, vortexed for 5 secs and
449 incubated on ice for 5 mins. After centrifugation at 500 x g for 5 mins at 4 °C, the supernatant was
450 collected as the cytosplasmic fraction. The pellet was resuspended in 500 µL of MIB buffer
451 (Membrane Isolation Buffer) from the kit, vortexed for 15 secs and incubated on ice for 5 mins.
452 After centrifugation at 8 000 x g for 5 mins at 4 °C, the supernatant was collected as the membrane
453 and organelles fraction. To each 100 µL of fraction was added 60 µL of loading buffer 1 x (from
454 ColdSpring Laemmli sample buffer: 50 mM Tris pH 6.8, 2 % SDS, 10 % Glycerol, 5 % β-
455 mercaptoethanol) before processing for western blot.

456 **Mitochondrial membrane potential measurements**

457 Mitochondrial membrane potential was measured by flow cytometry in HEK293 cells using TMRE
458 (Tetramethylrhodamine, Ethyl ester, Abcam, ab113852). FCCP was used as a positive control to
459 validate each independent experiment. Cells were grown up to 80 % confluence and washed twice
460 with PBS. The cells were then incubated for 5 mins at 37 °C, 5 % $CO_2$ with PBS/A (0.2 % BSA in PBS)
461 solution (experimental) or 3 µM FCCP in PBS/A solution (positive control). Then, 100 nM of TMRE
462 was added and cells were incubated 15 mins at 37 °C, 5 % $CO_2$. After incubation, cells were
463 trypsinized and centrifuged at 800 x g for 5 mins at 4 °C and resuspended in 500 µL of PBS and
464 kept on ice. Cells were immediately analysed by flow cytometry. A gate for living cells was set, as
465 well as a second gate to filter out cell doublets. TMRE fluorescence (PE-A) was recorded over a

466 minimum of 50 000 gated cells for each experimental condition. The mean TMRE fluorescence
467 intensity was measured over 3 independent experiments for each experimental condition.

468 **Stimulated Emission Depletion (STED) microscopy**

469 Samples were prepared as described above for confocal microscopy. A Leica TCS SP8 STED 3X was
470 used with a 100x objective lens and immersion oil for dual-color STED images. Images were
471 obtained by sequential scanning of a given area. The combination of Alexa Fluor 488 (Thermo
472 Fisher Scientific, A-11017) and Alexa Fluor 568 (Thermo Fisher Scientific, A-21069) dyes was
473 chosen for STED imaging. Alexa Fluor 488 dye was excited with a white light laser (WLL) at 488 nm
474 and was depleted using the 660 nm STED laser. Alexa Fluor 568 dye was excited with a WLL at
475 561 nm and was depleted using the 660 nm STED laser. The STED laser (660 nm) was applied at
476 80 % of maximum power.

477 **Fast Protein Liquid Chromatography (FPLC) and affinity-purification mass spectrometry (AP-MS)**

478 Mitochondrial extracts of HEK293 cells were centrifuged at 13 000 x g for 10 mins at 4 °C to
479 remove the supernatant and were resuspended in FPLC buffer (50 mM Tris-HCl, 1 mM EDTA, 150
480 mM NaCl, 1 % Triton X-100, pH 7.5, filtered with 0.2 µm filters) at 2 mg/mL for a total of 4 mg of
481 mitochondrial proteins. Samples were incubated on ice for 15 mins and then centrifuged at 10 000
482 x g for 5 mins at 4 °C and the supernatant was loaded in the injection syringe without disrupting
483 the pellet. The FPLC was performed on a HiLoad 16/60 Superdex 200 pg column (GE Healthcare,
484 Chicago, USA) at 4 °C. The column was pre-equilibrated with the FPLC buffer for up to 0.2 CV
485 (column volume) and the sample was applied at a flow rate of 0.5 mL/min with a pressure alarm
486 set at 0.5 MPa. The elution was performed over 72 fractions of 1.5 mL for a maximum of 1.1 CV.
487 For altFUS probing by western blot, proteins were precipitated from 150 µL of each 4 fractions in
488 technical duplicates. First, 600 µL of methanol was added to each tube and mixed gently, before
489 adding 150 µL of chloroform. Tubes were gently inverted 10 times before adding 450 µL of milliQ

490 $H_2O$ and vortexing briefly. After centrifugation at 12 000 x g for 3 mins, the upper phase was
491 discarded, and 400 µL of methanol was added. Tubes are centrifuged at 16 000 x g for 4 mins and
492 the pellet was resuspended in loading buffer. For interactome analysis by mass spectrometry,
493 fractions of interest (8 to 14) were pooled together and incubated at 4 °C overnight with magnetic
494 FLAG beads (Sigma, M8823) pre-conditioned with FPLC buffer. The beads were then washed 3
495 times with 5 mL of FPLC buffer, and 5 times with 5 mL of 20 mM $NH_4HCO_3$ (ABC). Proteins were
496 eluted and reduced from the beads using 10 mM DTT (15mins at 55 °C), and then treated with 20
497 mM IAA (1 hour at room temperature in the dark). Proteins were digested overnight by adding 1
498 µg of trypsin (Promega, Madison, Wisconsin) in 100 µL ABC at 37 °C overnight. Digestion was
499 quenched using 1 % formic acid and supernatant was collected. Beads were washed once with
500 acetonitrile/water/formic acid (1/1/0.01 v/v) and pooled with supernatant. Peptides were dried
501 with a speedvac, desalted using a C18 Zip-Tip (Millipore Sigma, Etobicoke, Ontario, Canada) and
502 resuspended into 30 µl of 1% formic acid in water prior to MS analysis.

503 **Mass-spectrometry analysis**

504 Peptides were separated in a PepMap C18 nano column (75 µm × 50 cm, Thermo Fisher Scientific).
505 The setup used a 0–35% gradient (0–215 min) of 90% acetonitrile, 0.1% formic acid at a flow rate
506 of 200 nL/min followed by acetonitrile wash and column re-equilibration for a total gradient
507 duration of 4 h with a RSLC Ultimate 3000 (Thermo Fisher Scientific, Dionex). Peptides were
508 sprayed using an EASYSpray source (Thermo Fisher Scientific) at 2 kV coupled to a quadrupole-
509 Orbitrap (QExactive, Thermo Fisher Scientific) mass spectrometer. Full-MS spectra within a m/z
510 350–1600 mass range at 70,000 resolution were acquired with an automatic gain control (AGC)
511 target of 1e6 and a maximum accumulation time (maximum IT) of 20 ms. Fragmentation (MS/MS)
512 of the top ten ions detected in the Full-MS scan at 17,500 resolution, AGC target of 5e5, a
513 maximum IT of 60 ms with a fixed first mass of 50 within a 3 m/z isolation window at a normalized

514 collision energy (NCE) of 25. Dynamic exclusion was set to 40 s. Mass spectrometry RAW files were
515 searched with Andromeda search engine implemented in MaxQuant 1.5.5.1. The digestion mode
516 was set at Trypsin/P with a maximum of two missed cleavages per peptides. Oxidation of
517 methionine and acetylation of N-terminal were set as variable modifications, and
518 carbamidomethylation of cysteine was set as fixed modification. Precursor and fragment
519 tolerances were set at 4.5 and 20 ppm respectively. Files were searched using a target-decoy
520 approach against UniprotKB (*Homo sapiens* 03/2017 release) with the addition of altFUS
521 sequence for a total of 92,949 entries. The false discovery rate (FDR) was set at 1% for peptide-
522 spectrum-match, peptide and protein levels. Protein interactions were then scored using the
523 SAINT algorithm, with Mock cells as control and the magnetic FLAG beads in HEK293 cells
524 crapome[63]. Proteins with a SAINT score above 0.99 were considered, as well as those presenting
525 a SAINT score above 0.88 with a minimum of two unique peptides.

526 **Biological processes and cellular compartment enrichment analysis**

527 Proteins identified in altFUS interactome were screened for cellular compartment and biological
528 processes enrichment using Gene Ontology (GO) enrichment. Proteins were queried against the
529 whole Human Proteome for cellular compartment and against the Human mitochondrial
530 proteome (MitoCarta 2.0) for biological processes. The statistical analysis used a Fisher's Exact
531 test with a FDR set at 1 %.

532 **Autophagic flux measurements**

533 The mCherry-GFP-LC3 was used to evaluate the autophagic vesicles within HeLa cells by confocal
534 microscopy. Before fusion with the lysosome, the LC3 molecules on the autophagosome display
535 a yellow fluorescence (combined mCherry and GFP fluorescence). After fusion, the GFP
536 fluorescence is quenched by the lysosomal pH, and as such the LC3 molecules display a red signal
537 (mCherry alone). This allows a visual representation of the autophagic flux in a given cell. Cells

538 treated with 50 nM Bafilomycin for 4 hours were used as a positive control to validate each
539 independent experiment. Observations were made across 2 technical duplicates for each
540 biological condition, across 3 independent experiments (n=3). Alternatively, the autophagic flux
541 was also evaluated by LC3 probing before and after bafilomycin treatment (50 nM for 4 hours).
542 The quantification corresponds to the treated / untreated ratio of LC3-II abundance.

543 **Cytoplasmic aggregates measurements**

544 Images of HeLa cells were taken by confocal microscopy and then processed using the Image J 3D
545 Objects Counter plugin. FUS cytoplasmic aggregates were then quantified in number and size
546 ($\mu m^2$) for each cell. A total of 100 cells across two technical replicates were taken for each
547 independent experiment (n=3, i.e. a minimum of 300 cells per biological conditions).

548 **Transgenic *Drosophila* and climbing assay**

549 The bicistronic constructs, FUS and FUS-R495x, and the monocistronic constructs, altFUS, $FUS^{(\emptyset)}$
550 and $FUS^{(\emptyset)}$-R495x, were subcloned in the pUASTattB expression vector for site specific insertion
551 into attP2 on chromosome 3. Transgenic flies were generated by Best Gene (Best Gene Inc.,
552 California, USA). The Elav-GeneSwitch-GAL4 driver (stock number: 43642, genotype: y[1] w[*];
553 P{w[+mC]=elav-Switch.O}GSG301) and the UAS-mCherry flies (stock number: 35787, genotype:
554 y[1] sc[*] v[1]; P{y[+t7.7] v[+t1.8]=UAS-mCherry.VALIUM10}attP2) was purchased from
555 Bloomington (Bloomington Drosophila Stock Center, Indiana, USA). All stocks were in a $w^{1118}$
556 background and were cultured on standard medium at 25°C or room temperature. Transgenic
557 flies were crossed with the Elav-GeneSwitch-GAL4 driver strain. The F1 was equally divided in two
558 groups with equal proportion of males and females: one group will feed on standard food
559 supplemented with ethanol (0.2 % - control flies), the other on standard food supplemented with
560 RU-486 at 10 µM diluted in ethanol (induced flies). The climbing assay was performed as
561 previously described[48]. Briefly, flies were transferred into an empty vial and tapped to the bottom.

562 After 18 s, the number of flies at the top of the tube were considered successful. The assay was
563 done at day 1, 10 and 20 post-induction, across 4 independent F1. Five flies were taken at day 1,
564 10 and 20 post-induction to validate expression of the proteins of interest.

565 **Statistical analyses and representation**

566 Unless otherwise stated, the statistical analysis carried was a two-way ANOVA with Tukey's
567 multiple comparison correction. The box plots represent the mean with the 5 to 95 % percentile.
568 The bar graphs represent the mean, and error bars correspond to the standard deviation. When
569 using parametric tests, normality of data distribution was verified beforehand using the Shapiro-
570 Wilk test.

571

572 **DATA AVAILABILITY STATEMENT**

573 The OpenProt database is available at www.openprot.org. The GTEx portal is available via
574 www.gtexportal.org. The Gwips portal is available at www.gwips.ucc.ie. The proteomics data are
575 available on the PRIDE repository with the accession PXD------ (**Fig 2l-m**). Any other relevant data
576 are available from the corresponding authors upon reasonable request.

577 **ACKNOWLEDGEMENTS**

578 This research was supported by CIHR grants MOP-137056 and MOP-136962, by an ALS Canada
579 Project Grant, and by a Canada Research Chair in Functional Proteomics and Discovery of Novel
580 Proteins to X.R. X.R and S.J are members of the Fonds de Recherche du Québec Santé (FRQS)-
581 supported Centre de Recherche du Centre Hospitalier Universitaire de Sherbrooke. P.M. is
582 supported by the ALS Double Play Christopher Chiu Postdoctoral Fellowship. We thank J. Ule, M-
583 J. Boucher and D. Hunting for helpful discussions. The autopsy program is supported by the James
584 Hunter and Family ALS Initiative. The Genotype-Tissue Expression (GTEx) Project was supported

585 by the Common Fund of the Office of the Director of the National Institutes of Health, and by NCI,
586 NHGRI, NHLBI, NIDA, NIMH, and NINDS. The data used for the analyses described in this
587 manuscript were obtained from the GTEx Portal on April 2019.

588 **CONTRIBUTIONS**

589 MA.B and X.R designed and wrote the study. MA.B and JF.J did the experiments, and MA.B did
590 the analyses and figures. S.N and S.J assisted with the Drosophila experiments. P.M, L.Z and J.R
591 provided the motor cortex tissue lysates. GE.T and R.P provided the iPSCs-derived motor neurons.
592 All authors proofread the manuscript.

593 **REFERENCES**


594 1. Morgan, S. & Orrell, R. W. Pathogenesis of amyotrophic lateral sclerosis. *Br. Med. Bull.* **119**,
595 87–98 (2016).
596 2. Mathis, S., Goizet, C., Soulages, A., Vallat, J.-M. & Masson, G. L. Genetics of amyotrophic
597 lateral sclerosis: A review. *J. Neurol. Sci.* **399**, 217–226 (2019).
598 3. Taylor, J. P., Brown Jr, R. H. & Cleveland, D. W. Decoding ALS: from genes to mechanism.
599 *Nature* **539**, 197–206 (2016).
600 4. Rosen, D. R. *et al.* Mutations in Cu/Zn superoxide dismutase gene are associated with familial
601 amyotrophic lateral sclerosis. *Nature* **362**, 59–62 (1993).
602 5. Nguyen, H. P., Broeckhoven, C. V. & Zee, J. van der. ALS Genes in the Genomic Era and their
603 Implications for FTD. *Trends Genet.* **0**, (2018).
604 6. Zou, Z.-Y., Liu, M.-S., Li, X.-G. & Cui, L.-Y. Mutations in FUS are the most frequent genetic
605 cause in juvenile sporadic ALS patients of Chinese origin. *Amyotroph. Lateral Scler. Front.*
606 *Degener.* **17**, 249–252 (2016).
607 7. Millecamps, S. *et al.* Phenotype difference between ALS patients with expanded repeats in
608 C9ORF72 and patients with mutations in other ALS-related genes. *J. Med. Genet.* **49**, 258–263
609 (2012).
610 8. Corcia, P. *et al.* A novel mutation of the C-terminal amino acid of FUS (Y526C) strengthens
611 FUS gene as the most frequent genetic factor in aggressive juvenile ALS. *Amyotroph. Lateral*
612 *Scler. Front. Degener.* 1–4 (2017) doi:10.1080/21678421.2016.1265564.
613 9. Deng, H., Gao, K. & Jankovic, J. The role of FUS gene variants in neurodegenerative diseases.
614 *Nat. Rev. Neurol.* **10**, 337–348 (2014).
615 10. Vance, C. *et al.* Mutations in FUS, an RNA Processing Protein, Cause Familial
616 Amyotrophic Lateral Sclerosis Type 6. *Science* **323**, 1208–1211 (2009).

617 11. Marrone, L. *et al.* FUS pathology in ALS is linked to alterations in multiple ALS-associated
618 proteins and rescued by drugs stimulating autophagy. *Acta Neuropathol. (Berl.)* (2019)
619 doi:10.1007/s00401-019-01998-x.
620 12. Dormann, D. *et al.* ALS-associated fused in sarcoma (FUS) mutations disrupt Transportin-
621 mediated nuclear import. *EMBO J.* **29**, 2841–2857 (2010).
622 13. Naumann, M. *et al.* Impaired DNA damage response signaling by FUS-NLS mutations
623 leads to neurodegeneration and FUS aggregate formation. *Nat. Commun.* **9**, 335 (2018).
624 14. Zou, Z.-Y. *et al.* Screening of the FUS gene in familial and sporadic amyotrophic lateral
625 sclerosis patients of Chinese origin. *Eur. J. Neurol.* **19**, 977–983 (2012).
626 15. Dini Modigliani, S., Morlando, M., Errichelli, L., Sabatelli, M. & Bozzoni, I. An ALS-
627 associated mutation in the FUS 3'-UTR disrupts a microRNA–FUS regulatory circuitry. *Nat.*
628 *Commun.* **5**, 4335 (2014).
629 16. Sabatelli, M. *et al.* Mutations in the 3' untranslated region of FUS causing FUS
630 overexpression are associated with amyotrophic lateral sclerosis. *Hum. Mol. Genet.* **22**, 4748–
631 4755 (2013).
632 17. Ajmone-Cat, M. A. *et al.* Increased FUS levels in astrocytes leads to astrocyte and
633 microglia activation and neuronal death. *Sci. Rep.* **9**, 4572 (2019).
634 18. Ju, S. *et al.* A Yeast Model of FUS/TLS-Dependent Cytotoxicity. *PLoS Biol.* **9**, (2011).
635 19. Chen, Y. *et al.* Expression of human FUS protein in Drosophila leads to progressive
636 neurodegeneration. *Protein Cell* **2**, 477–486 (2011).
637 20. Miguel, L. *et al.* Accumulation of insoluble forms of FUS protein correlates with toxicity
638 in Drosophila. *Neurobiol. Aging* **33**, 1008.e1–15 (2012).
639 21. Ling, S.-C. *et al.* Overriding FUS autoregulation in mice triggers gain-of-toxic dysfunctions
640 in RNA metabolism and autophagy-lysosome axis. *eLife* **8**, e40811 (2019).

641 22. Nolan, M., Talbot, K. & Ansorge, O. Pathogenesis of FUS-associated ALS and FTD: insights
642 from rodent models. *Acta Neuropathol. Commun.* **4**, (2016).
643 23. Samandi, S. *et al.* Deep transcriptome annotation enables the discovery and functional
644 characterization of cryptic small proteins. *eLife* **6**, e27860 (2017).
645 24. Saghatelian, A. & Couso, J. P. Discovery and characterization of smORF-encoded
646 bioactive polypeptides. *Nat. Chem. Biol.* **11**, 909–916 (2015).
647 25. Delcourt, V., Staskevicius, A., Salzet, M., Fournier, I. & Roucou, X. Small Proteins Encoded
648 by Unannotated ORFs are Rising Stars of the Proteome, Confirming Shortcomings in Genome
649 Annotations and Current Vision of an mRNA. *Proteomics* (2017)
650 doi:10.1002/pmic.201700058.
651 26. Brunet, M. A., Levesque, S. A., Hunting, D. J., Cohen, A. A. & Roucou, X. Recognition of
652 the polycistronic nature of human genes is critical to understanding the genotype-phenotype
653 relationship. *Genome Res.* (2018) doi:10.1101/gr.230938.117.
654 27. Brunet, M. A. *et al.* OpenProt: a more comprehensive guide to explore eukaryotic coding
655 potential and proteomes. *Nucleic Acids Res.* **47**, D403–D410 (2019).
656 28. Umoh, M. E. *et al.* A proteomic network approach across the ALS-FTD disease spectrum
657 resolves clinical phenotypes and genetic vulnerability in human brain. *EMBO Mol. Med.*
658 e201708202 (2017) doi:10.15252/emmm.201708202.
659 29. Collins, M. A., An, J., Hood, B. L., Conrads, T. P. & Bowser, R. P. Label-Free LC–MS/MS
660 Proteomic Analysis of Cerebrospinal Fluid Identifies Protein/Pathway Alterations and
661 Candidate Biomarkers for Amyotrophic Lateral Sclerosis. *J. Proteome Res.* **14**, 4486–4501
662 (2015).

663 30. Chick, J. M. *et al.* A mass-tolerant database search identifies a large proportion of
664 unassigned spectra in shotgun proteomics as modified peptides. *Nat. Biotechnol.* **33**, 743–
665 749 (2015).
666 31. Olexiouk, V., Van Criekinge, W. & Menschaert, G. An update on sORFs.org: a repository
667 of small ORFs identified by ribosome profiling. *Nucleic Acids Res.* **46**, D497–D502 (2018).
668 32. Zerbino, D. R. *et al.* Ensembl 2018. *Nucleic Acids Res.* **46**, D754–D761 (2018).
669 33. Michel, A. M., Kiniry, S. J., O'Connor, P. B. F., Mullan, J. P. & Baranov, P. V. GWIPS-viz:
670 2018 update. *Nucleic Acids Res.* **46**, D823–D830 (2018).
671 34. Pavesi, A. Asymmetric evolution in viral overlapping genes is a source of selective
672 protein adaptation. *Virology* **532**, 39–47 (2019).
673 35. Hall, C. E. *et al.* Progressive Motor Neuron Pathology and the Role of Astrocytes in a
674 Human Stem Cell Model of VCP-Related ALS. *Cell Rep.* **19**, 1739–1749 (2017).
675 36. Luisier, R. *et al.* Intron retention and nuclear loss of SFPQ are molecular hallmarks of
676 ALS. *Nat. Commun.* **9**, 1–15 (2018).
677 37. Carrì, M. T., D'Ambrosi, N. & Cozzolino, M. Pathways to mitochondrial dysfunction in ALS
678 pathogenesis. *Biochem. Biophys. Res. Commun.* **483**, 1187–1193 (2017).
679 38. Deng, J. *et al.* FUS Interacts with HSP60 to Promote Mitochondrial Damage. *PLOS Genet.*
680 **11**, e1005357 (2015).
681 39. Nakaya, T. & Maragkakis, M. Amyotrophic Lateral Sclerosis associated FUS mutation
682 shortens mitochondria and induces neurotoxicity. *Sci. Rep.* **8**, 15575 (2018).
683 40. Monahan, Z., Shewmaker, F. & Pandey, U. B. Stress granules at the intersection of
684 autophagy and ALS. *Brain Res.* **1649**, 189–200 (2016).
685 41. Aulas, A. & Vande Velde, C. Alterations in stress granule dynamics driven by TDP-43 and
686 FUS: a link to pathological inclusions in ALS? *Front. Cell. Neurosci.* **9**, (2015).

687 42. Hergesheimer, R. C. *et al.* The debated toxic role of aggregated TDP-43 in amyotrophic
688 lateral sclerosis: a resolution in sight? *Brain* **142**, 1176–1194 (2019).
689 43. Deng, H.-X. *et al.* FUS-immunoreactive inclusions are a common feature in sporadic and
690 non-SOD1 familial amyotrophic lateral sclerosis. *Ann. Neurol.* **67**, 739–748 (2010).
691 44. Tyzack, G. E. *et al.* Widespread FUS mislocalization is a molecular hallmark of
692 amyotrophic lateral sclerosis. *Brain J. Neurol.* (2019) doi:10.1093/brain/awz217.
693 45. Farrawell, N. E. *et al.* Distinct partitioning of ALS associated TDP-43, FUS and SOD1
694 mutants into cellular inclusions. *Sci. Rep.* **5**, 13416 (2015).
695 46. Lanson, N. A. *et al.* A Drosophila model of FUS-related neurodegeneration reveals
696 genetic interaction between FUS and TDP-43. *Hum. Mol. Genet.* **20**, 2510–2523 (2011).
697 47. Bogaert, E. *et al.* Molecular Dissection of FUS Points at Synergistic Effect of Low-
698 Complexity Domains in Toxicity. *Cell Rep.* **24**, 529-537.e4 (2018).
699 48. Chambers, R. P. *et al.* Nicotine increases lifespan and rescues olfactory and motor
700 deficits in a Drosophila model of Parkinson's disease. *Behav. Brain Res.* **253**, 95–102 (2013).
701 49. Kovacs, E., Tompa, P., Liliom, K. & Kalmar, L. Dual coding in alternative reading frames
702 correlates with intrinsic protein disorder. *Proc. Natl. Acad. Sci.* **107**, 5429–5434 (2010).
703 50. Pancsa, R. & Tompa, P. Coding Regions of Intrinsic Disorder Accommodate Parallel
704 Functions. *Trends Biochem. Sci.* **41**, 898–906 (2016).
705 51. Scekic-Zahirovic, J. *et al.* Toxic gain of function from mutant FUS protein is crucial to
706 trigger cell autonomous motor neuron loss. *EMBO J.* **35**, 1077–1097 (2016).
707 52. Delcourt, V. *et al.* The Protein Coded by a Short Open Reading Frame, Not by the
708 Annotated Coding Sequence, Is the Main Gene Product of the Dual-Coding Gene MIEF1. *Mol.
709 Cell. Proteomics MCP* **17**, 2402–2411 (2018).

710 53. Kino, Y. *et al.* FUS/TLS deficiency causes behavioral and pathological abnormalities
711 distinct from amyotrophic lateral sclerosis. *Acta Neuropathol. Commun.* **3**, (2015).
712 54. Hicks, G. G. *et al.* Fus deficiency in mice results in defective B-lymphocyte development
713 and activation, high levels of chromosomal instability and perinatal death. *Nat. Genet.* **24**,
714 175–179 (2000).
715 55. An, H. *et al.* ALS-linked FUS mutations confer loss and gain of function in the nucleus by
716 promoting excessive formation of dysfunctional paraspeckles. *Acta Neuropathol. Commun.* **7**,
717 7 (2019).
718 56. Al-Chalabi, A. & Hardiman, O. The epidemiology of ALS: a conspiracy of genes,
719 environment and time. *Nat. Rev. Neurol.* **9**, nrneurol.2013.203 (2013).
720 57. Qamar, S. *et al.* FUS Phase Separation Is Modulated by a Molecular Chaperone and
721 Methylation of Arginine Cation-π Interactions. *Cell* **173**, 720-734.e15 (2018).
722 58. Richards, S. *et al.* Standards and guidelines for the interpretation of sequence variants: a
723 joint consensus recommendation of the American College of Medical Genetics and Genomics
724 and the Association for Molecular Pathology. *Genet. Med. Off. J. Am. Coll. Med. Genet.* **17**,
725 405–424 (2015).
726 59. Bergeron, D. *et al.* An out-of-frame overlapping reading frame in the ataxin-1 coding
727 sequence encodes a novel ataxin-1 interacting protein. *J. Biol. Chem.* **288**, 21824–21835
728 (2013).
729 60. Vanderperre, B. *et al.* An overlapping reading frame in the PRNP gene encodes a novel
730 polypeptide distinct from the prion protein. *FASEB J.* **25**, 2373–2386 (2011).
731 61. Rathore, A. *et al.* MIEF1 Microprotein Regulates Mitochondrial Translation. *Biochemistry*
732 **57**, 5564–5575 (2018).

733 62. Peng, J.-Y. *et al.* Automatic Morphological Subtyping Reveals New Roles of Caspases in
734 Mitochondrial Dynamics. *PLOS Comput. Biol.* **7**, e1002212 (2011).
735 63. Choi, H. *et al.* SAINT: Probabilistic Scoring of Affinity Purification - Mass Spectrometry
736 Data. *Nat. Methods* **8**, 70–73 (2011).
737
738

739 **FIGURES' LEGEND**

740

741 **Figure 1: *FUS* is a bicistronic gene**

742 **a**, FUS gene bicistronic annotation, with the canonical FUS CDS (in blue, +1 frame) and altFUS CDS
743 (in green, +2 frame) represented on the FUS canonical transcript (*ENST00000254108* or
744 *NM_004960*). Sequence length proportions are respected, the scale bar corresponds to 300
745 nucleotides. **b**, *FUS* gene model, inspired from the GTEx portal, where exon combinations for the
746 five most abundant transcripts in the brain are represented below (sorted by decreasing
747 abundance). FUS CDS is coloured in blue, altFUS CDS is coloured in green, transcripts are identified
748 with Ensembl names (FUS-202: ENST00000380244; FUS-206: ENST00000487509; FUS-211:
749 ENST00000568901; FUS-203: ENST00000568901; FUS-201: ENST00000254108). **c**, RIBO-seq data
750 over the *FUS* gene (from the Gwips portal) with initiating ribosomes indicated in blue bars and
751 elongating ribosome footprints indicated with the blue curve. **d**, AltFUS protein conservation
752 across Human (*Homo sapiens*), Chimpanzee (*Pan troglodytes*), Rat (*Rattus norvegicus*), Mouse
753 (*Mus musculus*) and Dog (*Canis lupus familiaris*). Residues are coloured based on their degree of
754 conservation from white (none) to red (in all species). **e**, Mass spectrometry-based evidence for
755 altFUS protein with detected peptides indicated in grey and numbered according to **Extended**
756 **Data Table 1**. The peptide corresponding to the displayed MS/MS spectra below is indicated in
757 red (from re-analysis of PMID 26186194 by OpenProt). **f**, Expression of both FUS and altFUS from
758 the *FUS* construct in HEK293 cells by western blot, and expression of FUS with the monocistronic
759 construct $FUS^{(\emptyset)}$ (representative image from n=3). The western blot shows a low exposition
760 (endogenous FUS and altFUS non visible). **g**, AltFUS endogenous expression in HEK293 cells using
761 a siRNA targeting *FUS* mRNA as negative control and over-expression of altFUS CDS as positive
762 control (representative image from n=3). **h**, AltFUS (arrow) endogenous expression in Human
763 tissues (spinal cord, brain, muscles and kidney – 100 ug), in HEK293 and HeLa cultured cells (100
764 ug) and using the over-expression of altFUS CDS in HEK293 cells (50 ug) as positive control
765 (representative image from n=3). The asterisk indicates a protein species detected with the anti-
766 altFUS antibody specifically in the brain. **i**, **j,** AltFUS (arrow) endogenous expression in the motor
767 cortex of three C9orf72 and three sporadic ALS patients (**i**) or in iPSC-derived motor neurons of
768 three lines from controls and from ALS patients (**j**) (representative image from n=3). The asterisk
769 indicates a protein species detected with the anti-altFUS antibody specifically in the brain.

770

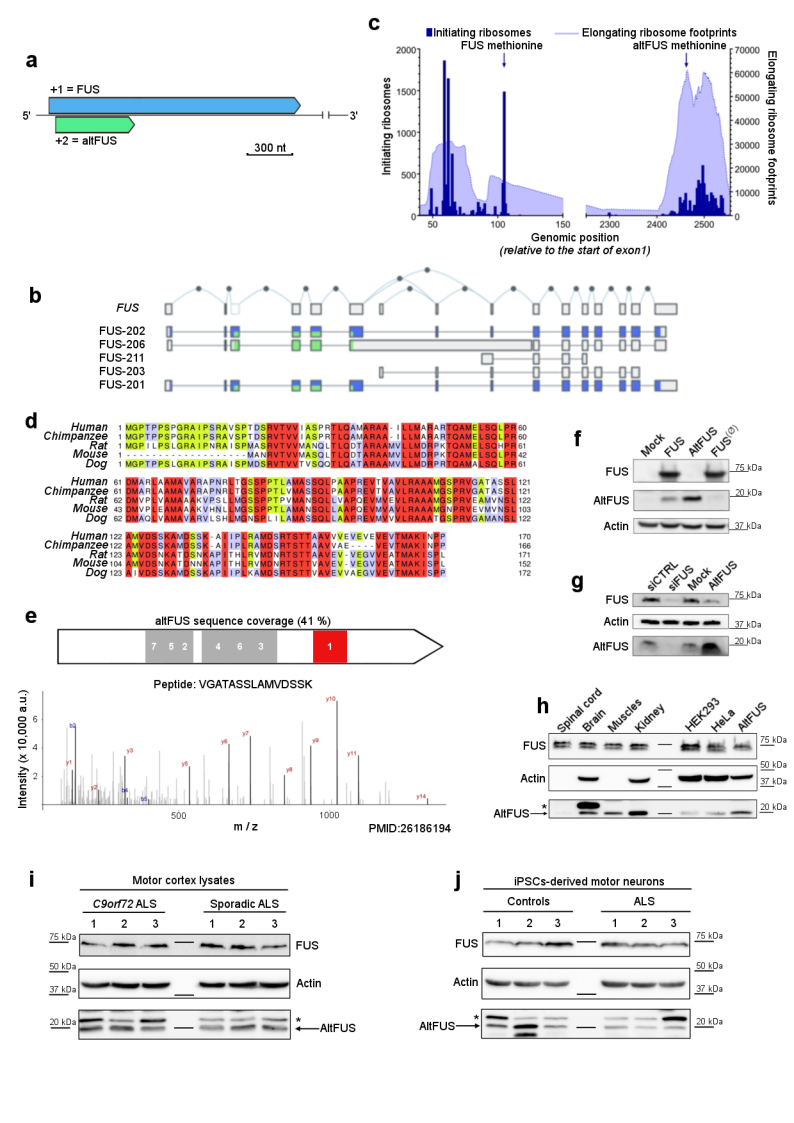
a
+1 = FUS
5'
3'
+2 = altFUS
300 nt
c
Initiating ribosomes
Elongating ribosome footprints
FUS methionine
altFUS methionine
Initiating ribosomes
Elongating ribosome footprints
Genomic position
(relative to the start of exon1)
b
FUS
FUS-202
FUS-206
FUS-211
FUS-203
FUS-201
d
Human
Chimpanzee
Rat
Mouse
Dog
e
altFUS sequence coverage (41 %)
Peptide: VGATASSLAMVDSSK
Intensity (x 10,000 a.u.)
m / z
PMID:26186194
f
Mock
FUS
AltFUS
FUS(D)
FUS
AltFUS
Actin
75 kDa
20 kDa
37 kDa
g
siCTRL
siFUS
Mock
AltFUS
FUS
Actin
AltFUS
75 kDa
37 kDa
20 kDa
h
Spinal cord
Brain
Muscles
Kidney
HEK293
HeLa
AltFUS
FUS
Actin
AltFUS
75 kDa
50 kDa
37 kDa
20 kDa
i
Motor cortex lysates
C9orf72 ALS
Sporadic ALS
1 2 3
1 2 3
75 kDa
50 kDa
37 kDa
20 kDa
FUS
Actin
AltFUS
j
iPSCs-derived motor neurons
Controls
ALS
1 2 3
1 2 3
FUS
Actin
AltFUS
75 kDa
50 kDa
37 kDa
20 kDa

771 **Figure 2: AltFUS is a mitochondrial protein involved in ALS-associated mitochondrial**
772 **dysfunction**

773 **a**, Images by confocal microscopy of altFUS-FLAG (green) in HeLa cells, using TOMM20 (red) as a
774 mitochondrial marker (representative image from n=3, Pearson's correlation r=0.92). The white
775 scale bar corresponds to 10µm. **b**, AltFUS-FLAG enrichment in mitochondrial extracts from
776 transfected HEK293 cells (representative image from n=3) with Hsp70 used as a mitochondrial
777 marker (WCL = Whole Cell Lysate, Mito = Mitochondria). **c**, AltFUS mitochondrial expression in
778 transfected HEK293 cells following fractionation (representative image from n=3), with Tubulin as
779 a cytosolic fraction marker and VDAC as a mitochondrial fraction marker (WCL = Whole Cell Lysate,
780 Cyto = Cytosol, Mito = mitochondria). **d**, Endogenous altFUS mitochondrial expression in HEK293
781 cells following fractionation (representative image from n=3), with Tubulin as a cytosolic fraction
782 marker and VDAC as a mitochondrial fraction marker, and with si*FUS* transfected cells as a
783 negative control and altFUS transfected cells as a positive control for altFUS expression (WCL =
784 Whole Cell Lysate, Cyto = Cytosol, Mito = mitochondria). **e**, Representative images of the
785 mitochondrial networks (TOMM20 in red) in mock and altFUS-FLAG (green) transfected HeLa cells
786 (n=3). The white scale bar corresponds to 10µm. **f**, Proportion of tubules and globules in the
787 mitochondrial network of mock and altFUS-FLAG transfected HeLa cells over a minimum of 100
788 cells across a technical duplicate per independent experiments (n=3, i.e. a minimum of 300 cells
789 per biological conditions, p value < 0.001, Mann-Whitney U test). **g**, Representative traces of
790 TMRE fluorescence measured by flow cytometry in mock cells and cells overexpressing the
791 bicistronic FUS-R495x or the monocistronic $FUS^{(\emptyset)}$-R495x constructs (n=4, minimum of 50 000 live
792 cells per independent replicates). Mean fluorescence intensity of mock cells treated with the
793 decoupling agent, FCCP, is indicated with a grey dotted line. **h**, Mean TMRE fluorescence intensity
794 measures in mock cells, cells over-expressing altFUS, FUS, $FUS^{(\emptyset)}$, FUS-R495x or $FUS^{(\emptyset)}$-R495x, or
795 mock cells treated with FCCP across 3 independent experiments (n=4). Statistical significance is
796 relative to the mock condition unless otherwise indicated (*** = p value < 0.001, **** = p value
797 < 0.0001, ns = non-significant). **i**, Representative image by stimulated emission depletion
798 microscopy (STED) of altFUS-FLAG (green) localization within mitochondria (TOMM20 marker in
799 red). The white bar across the mitochondria represents the region of interest quantified in panel
800 **j**. The white scale bar corresponds to 3µm. **j**, Relative fluorescence histogram for altFUS-FLAG and
801 TOMM20 across the region of interest highlighted by a white line on panel **i**. **k**, AltFUS expression
802 in fractions following size exclusion chromatography on HEK293 cells mitochondrial extracts
803 (representative image from n=2). **l**, Predicted localisations of proteins identified in altFUS-FLAG
804 affinity purification-mass spectrometry (AP-MS) from fractions 8 to 14 after size exclusion
805 chromatography (**k**) on HEK293 cells mitochondrial extracts (n=2, confident identifications with a
806 SAINT score > 0.85 across 2 independent experiments). **m**, Enrichment of biological processes in
807 altFUS interacting proteins compared to the Human mitochondrial proteome (n=2, Fisher's Exact
808 test with FDR < 0.1 %).

809

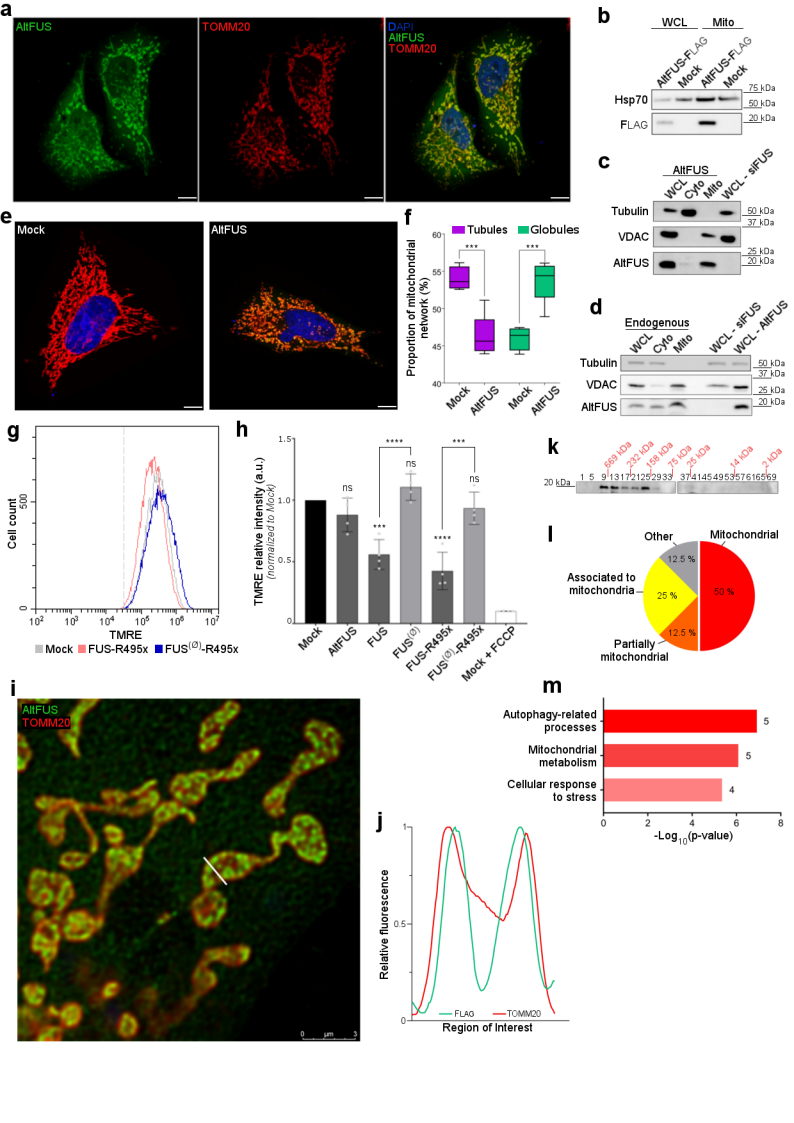
a
AltFUS
TOMM20
DAPI
AltFUS
TOMM20
b
WCL
Mito
AltFUS-FLAG
Mock
AltFUS-FLAG
Mock
Hsp70
FLAG
75 kDa
50 kDa
20 kDa
c
AltFUS
WCL
Cyto
Mito
WCL - siFUS
Tubulin
VDAC
AltFUS
50 kDa
37 kDa
25 kDa
20 kDa
d
Endogenous
WCL
Cyto
Mito
WCL - siFUS
WCL - AltFUS
Tubulin
VDAC
AltFUS
50 kDa
37 kDa
25 kDa
20 kDa
e
Mock
AltFUS
f
Tubules
Globules
Proportion of mitochondrial network (%)
60
55
50
45
40
***
***
Mock
AltFUS
Mock
AltFUS
g
Cell count
500
0
TMRE
Mock
FUS-R495x
FUS(S)-R495x
h
TMRE relative intensity (a.u.)
(normalized to Mock)
1.5
1.0
0.5
0
****
***
****
ns
ns
ns
***
Mock
AltFUS
FUS
FUS(S)
FUS-R495x
FUS(S)-R495x
Mock + FCCP
k
569 kDa
232 kDa
159 kDa
75 kDa
35 kDa
14 kDa
2 kDa
20 kDa
1 5 9 13 17 21 26 29 33 37 41 45 49 53 57 61 65 69
l
Other
Mitochondrial
Associated to mitochondria
Partially mitochondrial
12.5 %
50 %
25 %
12.5 %
i
AltFUS
TOMM20
0 µm 3
m
Autophagy-related processes
Mitochondrial metabolism
Cellular response to stress
5
5
4
0
2
4
6
8
-Log10(p-value)
j
Relative fluorescence
1
0.5
0
FLAG
TOMM20
Region of Interest

810 **Figure 3: AltFUS is necessary for ALS-associated inhibition of autophagy and accumulation of**
811 **FUS/TDP-43 cytoplasmic aggregates**

812 **a**, Images by confocal microscopy of mCherry-GFP-LC3 signal in HeLa cells across biological
813 conditions: untreated mock, bafilomycin treated mock, altFUS, FUS, FUS$^{(Ø)}$, FUS-R495x and FUS$^{(Ø)}$-
814 R495x (representative images of n=3). The white scale bar corresponds to 10µm and the zoomed
815 in region (right panel) is delimited as a white box. **b**, LC3-II accumulation after bafilomycin
816 treatment from mock, altFUS, FUS, FUS$^{(Ø)}$, FUS-R495x, FUS$^{(Ø)}$-R495x transfected cells and FUS$^{(Ø)}$-
817 R495x and altFUS co-transfected cells across 3 independent experiments (n=3). The quantification
818 corresponds to the treated/untreated ratio of LC3-II abundance. Statistical significance is relative
819 to the mock condition unless otherwise indicated (**** = p value < 0.0001, *** = p value < 0.001,
820 ** = p value < 0.01, ns = non-significant). **c**, Images by confocal microscopy of altFUS (FLAG tagged-
821 white), FUS (GFP tagged - green) and TDP-43 (red) signals in HeLa cells transfected with the
822 bicistronic GFP-FUS$^{(FLAG)}$-R495x or the monocistronic GFP-FUS$^{(Ø\text{-}FLAG)}$-R4955x constructs, or co-
823 transfected with the monocistronic GFP-FUS$^{(Ø\text{-}FLAG)}$-R495x and altFUS-FLAG constructs
824 (representative images from n=3). The white scale bar corresponds to 10µm. **d-e**, Quantification
825 of FUS cytoplasmic granules, number (**d**) and area (µm$^2$) (**e**) in cells over-expressing the bicistronic
826 (+) or monocistronic (-) construct for FUS, FUS-G156E, FUS-R495x, FUS-K510E, FUS-Q519x, FUS-
827 Q519I-fs527x, FUS-R521C, and FUS-P525L. Statistical comparisons are made between bicistronic
828 and monocistronic versions of each construct (**** = p value < 0.0001, *** = p value < 0.001, **
829 = p value < 0.01, * = p value < 0.05, ns = non-significant, one-way ANOVA test with Sidak's multiple
830 comparison).

831

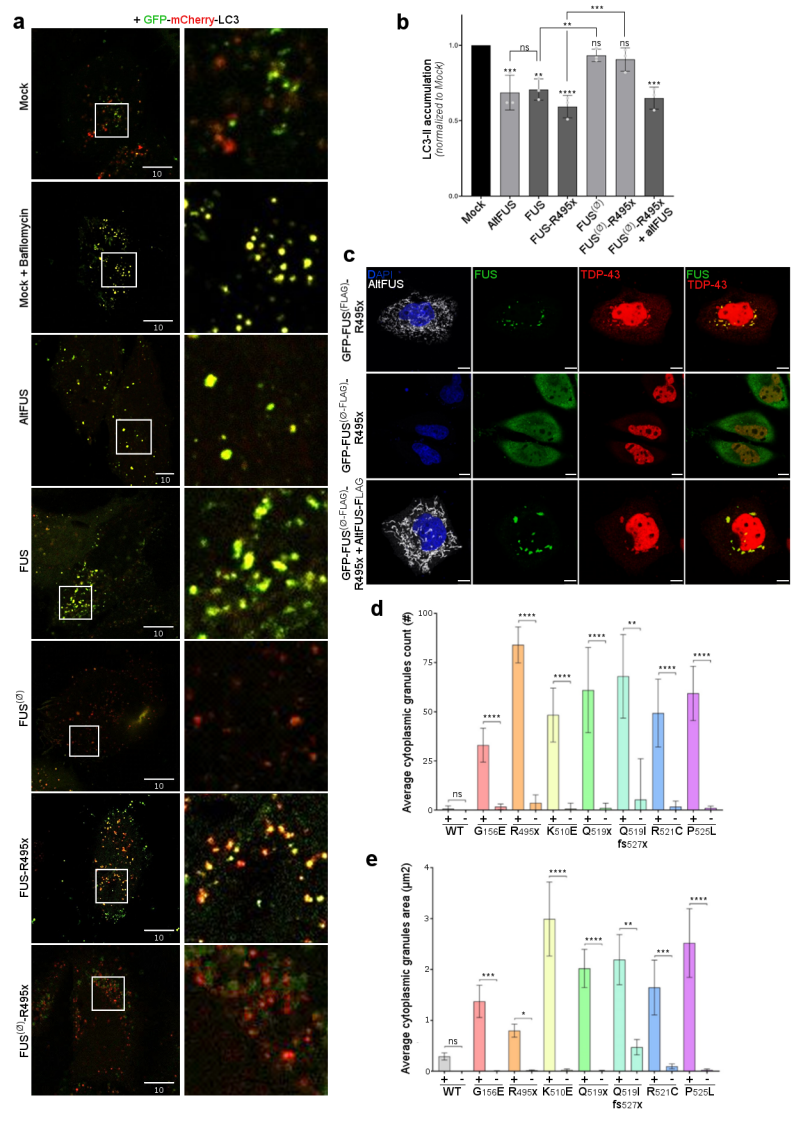
a
+ GFP-mCherry-LC3
Mock
Mock + Bafilomycin
AltFUS
FUS
FUS(Δ)
FUS-R495x
FUS(Δ)-R495x
10
b
LC3-II accumulation
(normalized to Mock)
1.0
0.5
0.0
ns
***
**
****
Mock
AltFUS
FUS
FUS-R495x
FUS(Δ)
FUS(Δ)-R495x
FUS(Δ)-R495x + altFUS
c
DAPI
AltFUS
FUS
TDP-43
FUS
TDP-43
GFP-FUS(FLAG)-R495x
GFP-FUS(Δ-FLAG)-R495x
GFP-FUS(Δ-FLAG)-R495x + AltFUS-FLAG
d
Average cytoplasmic granules count (#)
100
75
50
25
0
ns
****
**
WT
G156E
R495X
K510E
Q519X
Q519I
R521C
P525L
fs527X
e
Average cytoplasmic granules area (µm2)
4
3
2
1
0
ns
*
***
**
****

832 **Figure 4: AltFUS expression is necessary for the full *FUS*-linked ALS phenotype in *Drosophila***

833 **a**, Cross-breeding strategy for *Drosophila* generation using the Elav-GeneSwitch-GAL driver as an
834 inducible expression system specific to the motoneurons. **b**, FUS and altFUS expression in
835 mCherry (control), altFUS, FUS, FUS$^{(\emptyset)}$, FUS-R495x or FUS$^{(\emptyset)}$-R495x expressing *Drosophila* from the
836 control F1 and the RU-486 treated F1 (**a**) at 1, 10 or 20 days post-induction (representative image
837 from n=2). **c-e**, Locomotion assay using percentage of climbing success in control and RU-486-
838 treated transgenic *Drosophila* expressing mCherry or altFUS (**c**), the bicistronic FUS or the
839 monocistronic FUS$^{(\emptyset)}$ (**d**), and the bicistronic FUS-R495x or the monocistronic FUS$^{(\emptyset)}$-R495x (**e**) at
840 day 1, 10 and 20 post-induction. Statistical comparison were made between each population
841 (n=4). Indicated significance are between the monocistronic and the bicistronic transgenic flies of
842 the RU-486-treated population (ns = non-significant, * = p value < 0.05, *** = p value < 0.001).

843

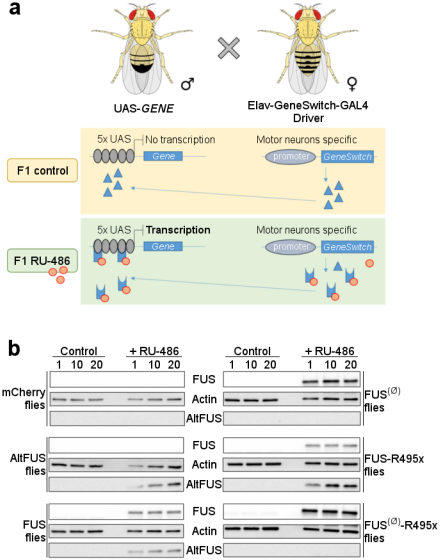
a
UAS-GENE
Elav-GeneSwitch-GAL4 Driver
F1 control
5x UAS
No transcription
Gene
Motor neurons specific
promoter
GeneSwitch
F1 RU-486
5x UAS
Transcription
Gene
Motor neurons specific
promoter
GeneSwitch
b
Control
+ RU-486
1 10 20
mCherry flies
AltFUS flies
FUS flies
FUS
Actin
AltFUS
FUS(Ø) flies
FUS-R495x flies
FUS(Ø)-R495x flies

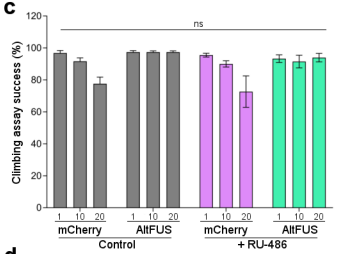
c
ns
Climbing assay success (%)
mCherry
AltFUS
mCherry
AltFUS
Control
+ RU-486

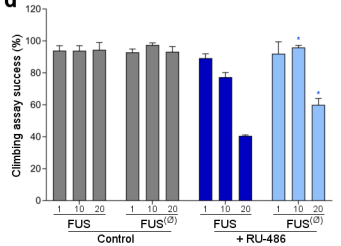
d
Climbing assay success (%)
FUS
FUS(Ø)
FUS
FUS(Ø)
Control
+ RU-486

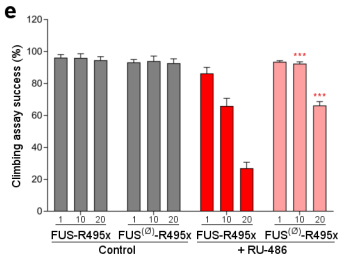
e
Climbing assay success (%)
FUS-R495x
FUS(Ø)-R495x
FUS-R495x
FUS(Ø)-R495x
Control
+ RU-486

844 **Figure 5: FUS mutations, synonymous for FUS but missense for altFUS, potentiate TDP-43**
845 **cytoplasmic aggregation**

846 **a**, Graphical representation of *FUS* mutations found in ALS patients, that are synonymous (dark
847 blue) for FUS protein (blue) but missense (red) for altFUS protein (green), on the canonical FUS
848 mRNA (*ENST00000254108* or *NM_004960*). **b**, Images by confocal microscopy of altFUS (FLAG
849 tagged - green) and mitochondria (TOMM20 marker, red) in HeLa cells over-expressing altFUS-
850 FLAG, altFUS-P31L-FLAG, altFUS-A38V-FLAG, altFUS-A46V-FLAG or altFUS-R64P-FLAG constructs
851 (representative images from n=3). Deconvolution over a maximum of 30 iterations on the green
852 and red channels was performed for the zoomed in pictures (the zoomed in regions are
853 highlighted in white). The white scale bar corresponds to 10µm. **c**, Images by confocal microscopy
854 of TDP-43 (yellow), FUS (GFP tagged - green) and altFUS (FLAG tagged - red) in HeLa cells over-
855 expressing GFP-FUS$^{(FLAG)}$, GFP-FUS$^{(P31L-FLAG)}$-S44=, GFP-FUS$^{(A38V-FLAG)}$-G51=, GFP-FUS$^{(A46V-FLAG)}$-G59= or
856 GFP-FUS$^{(R64P-FLAG)}$-S77= constructs (representative images from n=3). The white scale bar
857 corresponds to 10µm. **d**, Quantification of cells with TDP-43 aggregates in HeLa cells from (**c**),
858 where the data are represented as the fold-change compared to the GFP-FUS$^{(FLAG)}$ expressing cells.
859 Statistical significance is indicated above the bars (n=3, **** = p value < 0.0001).

860

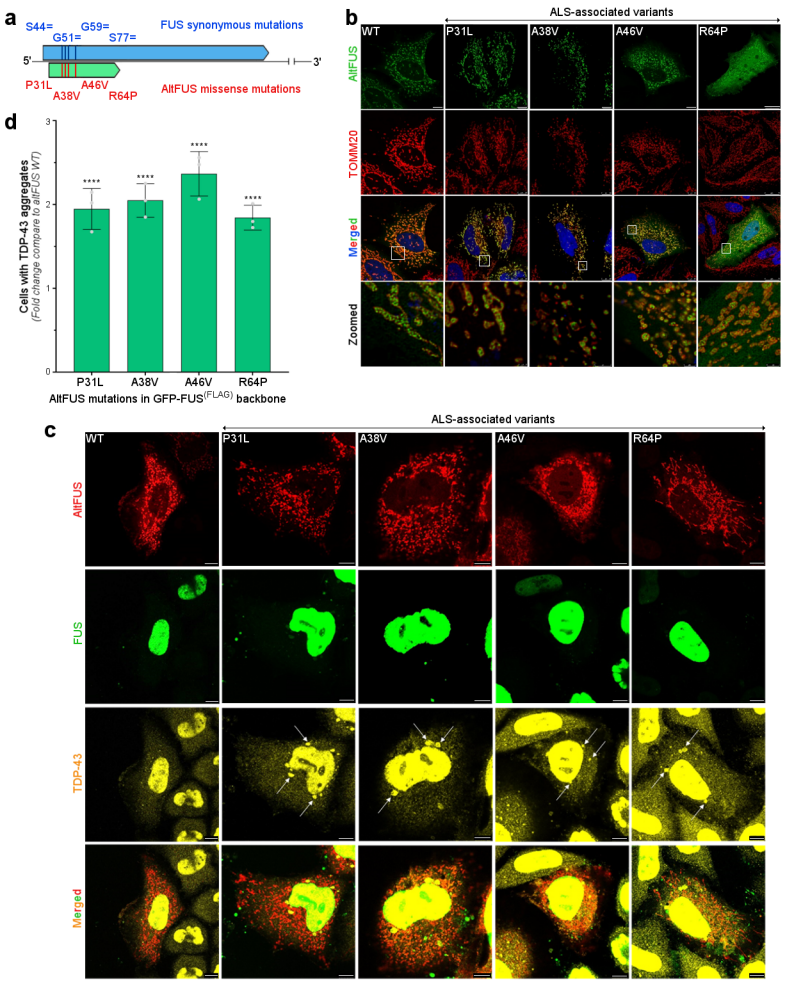
a
S44=
G51=
G59=
S77=
FUS synonymous mutations
5'
3'
P31L
A38V
A46V
R64P
AltFUS missense mutations
b
ALS-associated variants
WT
P31L
A38V
A46V
R64P
AltFUS
TOMM20
Merged
Zoomed
d
Cells with TDP-43 aggregates
(Fold change compare to altFUS WT)
****
P31L
A38V
A46V
R64P
AltFUS mutations in GFP-FUS(FLAG) backbone
c
ALS-associated variants
WT
P31L
A38V
A46V
R64P
AltFUS
FUS
TDP-43
Merged

861 **Extended Data - Legend**

862 For: *FUS* gene is dual-coding with both proteins united in molecular hallmarks of amyotrophic
863 lateral sclerosis, Brunet MA, *et al*.

864 **Extended Data Table 1**

865 OpenProt search results for FUS transcripts *ENST00000254108* and *NM_004960.3*. The OpenProt
866 version 1.3 was used. Each protein prediction is identified with a unique protein accession
867 (starting with II_ for novel predicted isoform, and IP_ for predicted alternative proteins). All
868 predicted alternative proteins are coloured in light blue. The protein localization is relative to the
869 canonical FUS coding sequence (CDS). The furthered studied protein, named altFUS (IP_243680)
870 is highlighted in dark blue. The workbook also contains the list of peptides identified in re-analysis
871 of mass spectrometry experiments using the OpenProt database (version 1.3).

872 **Extended Data Table 2**

873 AltFUS conservation across vertebrates. The workbook contains the list of *FUS* transcripts
874 retrieved from NCBI RefSeq database (transcript accession and nucleotidic sequences); the list of
875 transcripts containing an altFUS sequence (transcript accession, species, and altFUS protein
876 sequence); and the matrix of altFUS protein sequence identity between each species.

877 **Extended Data Alignment File**

878 Alignment of altFUS protein sequences across all 82 species. The alignment was done using
879 Clustalω, and coloured based on conservation from white (highly variable residue) to dark blue
880 (highly conserved residue).

881 **Extended Data Table 3**

882 Proteins identified by mass spectrometry following size exclusion chromatography (FPLC) and
883 FLAG affinity purification on mitochondrial extracts from HEK293 cells over-expressing altFUS-
884 FLAG. The proteins are listed by their UniProtKB accession alongside their annotated function, the
885 number of unique peptides supporting the detection and the number of peptide spectrum
886 matches (PSMs) within each experimental condition. Confidence of the interaction was scored
887 using the SAINT algorithm. The SAINT score is also reported.

888 **Extended Data Table 4**

889 *FUS* mutations, synonymous for FUS but missense for altFUS. The first sheet contains mutations
890 identified from a manually curated literature review. The second sheet retrieves variants in sALS
891 cases from the ALS Variant Server (http://als.umassmed.edu/). The third sheet retrieves variants
892 in fALS cases from the ALS Variant Server.

893 **Extended Data Table 5**

894 16 ALS-associated genes with currently non-annotated proteins detected in OpenProt database.
895 The OpenProt version 1.3 was used. The workbook contains the list of novel predicted proteins
896 from these genes, which have already be detected by mass spectrometry or ribosome profiling.

897

898 **Extended Data Figure 1**

899 **a**, AltFUS is encoded within an alternative open reading frame (ORF) overlapping the FUS
900 canonical CDS. When read in the +1 frame, the *FUS* mRNA (here *NM_004960.3*) codes for a 526
901 amino acid protein (highlighted in blue), named FUS. In the +2 frame, the *FUS* mRNA contains a
902 second ORF (highlighted in green) that codes for a novel 170 amino acid protein, named altFUS.
903 The two proteins are not isoforms. **b**, GTEx portal data on *FUS* mRNA expression in ALS-related
904 tissues are shown in blue colored scale. Transcripts are identified with Ensembl accessions (the
905 number after the dot corresponds to the version used in the analysis) and are quantified across
906 14 tissues. Five transcripts share 85 % of all mRNA expression level (framed in red). **c**, Table
907 compiling protein information relayed by Ensembl and OpenProt databases for the afore-
908 mentioned transcripts. The FUS protein is highlighted in blue. The altFUS protein is highlighted in
909 green. **d**, RIBO-seq data from the Gwips portal in *Mus musculus* shows an accumulation of initiating
910 ribosomes at the FUS methionine and the altFUS methionine (green bars). Elongating ribosomes
911 footprints density increase in the bicistronic region (light green curve). Data corresponds to global
912 aggregates across the studies supported by Gwips. **e**, PhyloP nucleotidic conservation scores are
913 represented in grey across the *FUS* mRNA (FUS-201), and in blue after noise reduction (Fast
914 Fourrier Transformation). The average PhyloP score on the bicistronic and the monocistronic
915 region are represented as a dotted red line. The FUS CDS is represented by a blue box, the altFUS
916 CDS is represented by the green box. **f**, Heatmap of altFUS protein sequences identity across 84
917 species. Primates, Rodents and Mammals in general display a strong protein conservation. The
918 sequence identity is colored from blue (0 %) to red (100 %).

919

**a**

**>FUS – NM_004960.3**

ACTTAAGCTTCGACGCAGGAGGCGGGGCTGCTCAGTCCTCCAGGCGTCGGTACTCAGCGGTGTTGGAACTTCGTTGCTTGCTTG
CCTGTGCGCGCGTGCGCGGAC**ATG**GCCTCAAACGATTATACCCAACAAGCAACCCAAAGCT***ATG***GGGCCTACCCCACCCAGCCC
GGGCAGGGCTATTCCCAGCAGAGCAGTCAGCCCTACGGACAGCAGAGTTACAGTGGTTATAGCCAGTCCACGGACACTTCAGGC
TATGGCCAGAGCAGCTATTCTTCTTATGGCCAGAGCCAGAACACAGGCTATGGAACTCAGTCAACTCCCCAGGGATATGGCTCGAC
TGGCGGCTATGGCAGTAGCCAGAGCTCCCAATCGTCTTACGGGCAGCAGTCCTCCTACCCTGGCTATGGCCAGCAGCCAGCTCC
CAGCAGCACCTCGGGAAGTTACGGTAGCAGTTCTCAGAGCAGCAGCTATGGGCAGCCCCAGAGTGGGAGCTACAGCCAGCAGC
CTAGCTATGGTGGACAGCAGCAAAGCTATGGACAGCAGCAAAGCTATAATCCCCCTCAGGGCTATGGACAGCAGAACCAGTACAA
CAGCAGCAGTGGTGGTGGAGGTGGAGGTGGAGGTGGAGGTAACTATGGCCAAGATCAATCCTCCA**TGA**GTAGTGGTGGTGGCA
GTGGTGGCGGTTATGGCAATCAAGACCAGAGTGGTGGAGGTGGCAGCGGTGGCTATGGACAGCAGGACCGTGGAGGCCGCGG
CAGGGGTGGCAGTGGTGGCGGCGGCGGCGGCGGCGGTGGTGGTTACAACCGCAGCAGTGGTGGCTATGAACCCAGAGGTCGT
GGAGGTGGCCGTGGAGGCAGAGGTGGCATGGGCGGAAGTGACCGTGGTGGCTTCAATAAATTTGGTGGCCCTCGGGACCAAG
GATCACGTCATGACTCCGAACAGGATAATTCAGACAACAACACCATCTTTGTGCAAGGCCTGGGTGAGAATGTTACAATTGAGTCT
GTGGCTGATTACTTCAAGCAGATTGGTATTATTAAGACAAACAAGAAAACGGGACAGCCCATGATTAATTTGTACACAGACAGGGAA
ACTGGCAAGCTGAAGGGAGAGGCAACGGTCTCTTTTGATGACCCACCTTCAGCTAAAGCAGCTATTGACTGGTTTGATGGTAAAG
AATTCTCCGGAAATCCTATCAAGGTCTCATTTGCTACTCGCCGGGCAGACTTTAATCGGGGTGGTGGCAATGGTCGTGGAGGCCG
AGGGCGAGGAGGACCCATGGGCCGTGGAGGCTATGGAGGTGGTGGCAGTGGTGGTGGTGGCCGAGGAGGATTTCCCAGTGGA
GGTGGTGGCGGTGGAGGACAGCAGCGAGCTGGTGACTGGAAGTGTCCTAATCCCACCTGTGAGAATATGAACTTCTCTTGGAGG
AATGAATGCAACCAGTGTAAGGCCCCTAAACCAGATGGCCCAGGAGGGGGACCAGGTGGCTCTCACATGGGGGGTAACTACGGG
GATGATCGTCGTGGTGGCAGAGGAGGCTATGATCGAGGCGGCTACCGGGGCCGCGGCGGGGACCGTGGAGGCTTCCGAGGGG
GCCGGGGTGGTGGGGACAGAGGTGGCTTTGGCCCTGGCAAGATGGATTCCAGGGGTGAGCACAGACAGGATCGCAGGGAGAG
GCCGTAT**TAA**TTAGCCTGGCTCCCCAGGTTCTGGAACAGCTTTTT [....]GTAAGAA

**Frame +1 = FUS protein**

MASNDYTQQATQSYGAYPTQPGQGYSQQSSQPYGQQSYSGYSQSTDTSGYGQSSYSSYGQSQNTGYGTQSTPQGYGSTGGYGS
SQSSQSSYGQQSSYPGYGQQPAPSSTSGSYGSSSQSSSYGQPQSGSYSQQPSYGGQQQSYGQQQSYNPPQGYGQQNQYNSSS
GGGGGGGGGGNYGQDQSSMSSGGGSGGGYGNQDQSGGGGSGGYGQQDRGGRGRGGSGGGGGGGGGGYNRSSGGYEPRGR
GGGRGGRGGMGGSDRGGFNKFGGPRDQGSRHDSEQDNSDNNTIFVQGLGENVTIESVADYFKQIGIIKTNKKTGQPMINLYTDRETG
KLKGEATVSFDDPPSAKAAIDWFDGKEFSGNPIKVSFATRRADFNRGGGNGRGGRGRGGPMGRGGYGGGGSGGGGRGGFPSGGG
GGGGQQRAGDWKCPNPTCENMNFSWRNECNQCKAPKPDGPGGGPGGSHMGGNYGDDRRGGRGGYDRGGYRGRGGDRGGFR
GGRGGGDRGGFGPGKMDSRGEHRQDRRERPY

**Frame +2 = altFUS protein**

MGPTPPSPGRAIPSRAVSPTDSRVTVVIASPRTLQAMARAAILLMARARTQAMELSQLPRDMARLAAMAVARAPNRLTGSSPPTLAMAS
SQLPAAPREVTVAVLRAAAMGSPRVGATASSLAMVDSSKAMDSSKAIIPLRAMDSRTSTTAAVVVEVEVEVEVTMAKINPP

**b**

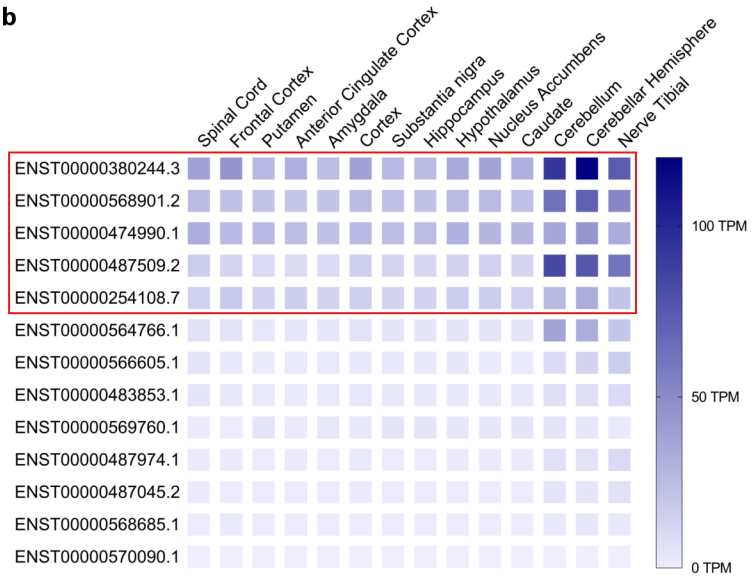


**c**

| Transcript | Ensembl Protein Information | OpenProt Protein Information |
|---|---|---|
| ENST00000380244 (FUS-202) | **ENSP00000369594** 525 amino acids (FUS isoform) | **ENSP00000369594** 525 amino acids (FUS isoform) |
| | | **IP_243691** 169 amino acids (IP_243680 isoform) |
| ENST00000487509 (FUS-206) | **No Protein** | **IP_243680** 170 amino acids |
| ENST00000568901 (FUS-211) | **No Protein** | **No Protein** |
| ENST00000474990 (FUS-203) | **No Protein** | **No Protein** |
| ENST00000254108 (FUS-201) | **ENSP00000254108** 526 amino acids (FUS) | **ENSP00000254108** 526 amino acids (FUS) |
| | | **IP_243680** 170 amino acids |

**d**

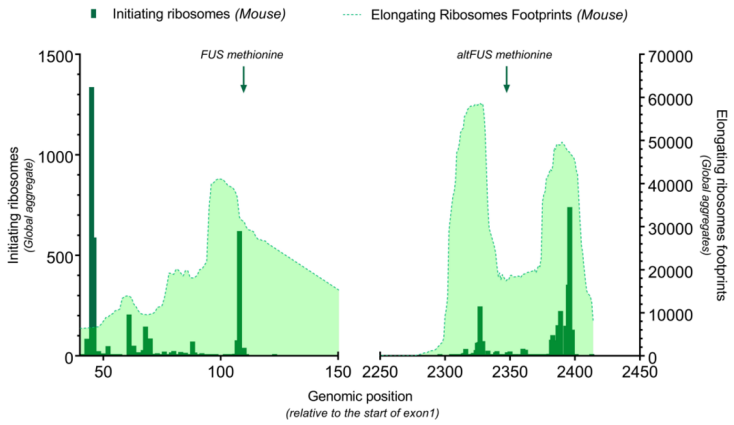


**e**

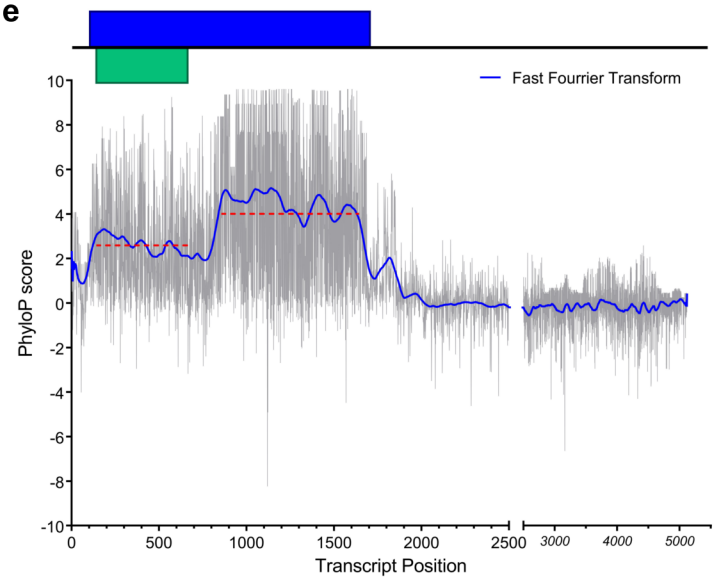


**f**

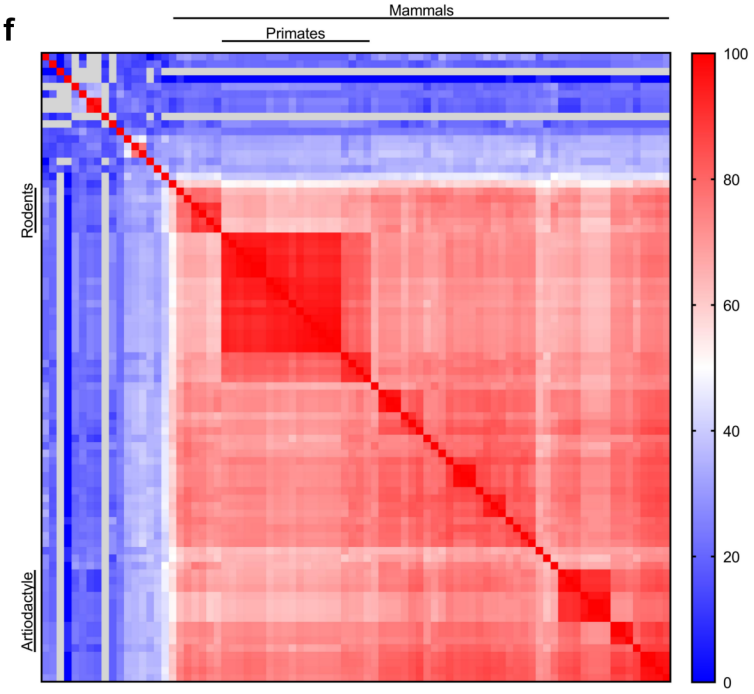

920 **Extended Data Figure 2**

921 **a**, AltFUS custom antibody strategy, with epitopes highlighted in bold on altFUS sequence (green),
922 and ELISA test results on both bleeds from each rabbits. **b**, Nucleotidic mutations on *FUS* mRNA
923 (*NM_004960*) are highlighted in red and mutate all altFUS methionines to threonines (altFUS_Ø).
924 **c-d**, Protein alignment of altFUS (**c**) and FUS (**d**) proteins from FUS bicistronic construct and the
925 monocistronic ($FUS^{(Ø)}$) construct, residues are coloured based on sequence identity (dark blue for
926 identical residues).

927

**a**

MGPT**PPSPGRAIPSRAVSPTDSR**VTVVIASPRTLQAMARAAILLMARARTQAMELSQLPRDMARLAAMAVA**RAPNRLTGSSPPTLA**MASSQLPAAPREVTVAVLRA
AAMGSPRVGATASSLAMVDSSKAMDSSKAIIPLRAMDSRTSTTAAVVVEVEVEVEVTMAKINPP

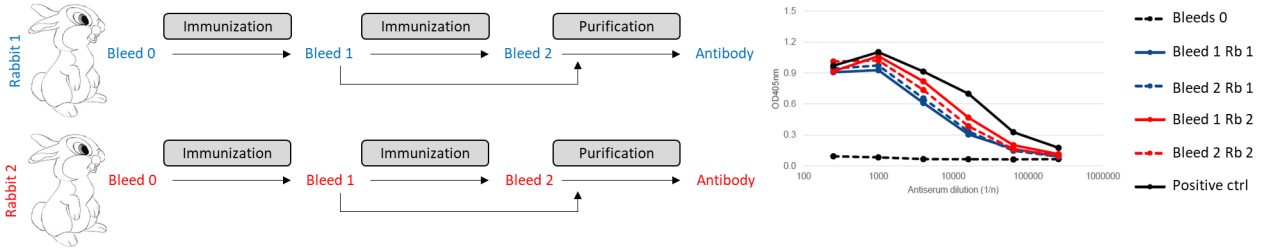


**b**

**>Mutated_sequence**

**ACG**GGGCCTACCCCACCCAGCCCGGGCAGGGCTATTCCCAGCAGAGCAGTCAGCCCTACGGACAGCAGAGTTACAGTGGTTATAGC
CAGTCCACGGACACTTCAGGCT**ACG**GCCAGAGCAGCTATTCTTCTT**ACG**GCCAGAGCCAGAACACAGGCT**ACG**GAACTCAGTCAAC
TCCCCAGGGAT**ACG**GCTCGACTGGCGGCT**ACG**GCAGTAGCCAGAGCTCCCAATCGTCTTACGGGCAGCAGTCCTCCTACCCTGGCT**A**
**CG**GCCAGCAGCCAGCTCCCAGCAGCACCTCGGGAAGTTACGGTAGCAGTTCTCAGAGCAGCAGCT**ACG**GGCAGCCCCAGAGTGGG
AGCTACAGCCAGCAGCCTAGCT**ACG**GTGGACAGCAGCAAAGCT**ACG**GACAGCAGCAAAGCTATAATCCCCCTCAGGGCT**ACG**GACA
GCAGAACCAGTACAACAGCAGCAGTGGTGGTGGAGGTGGAGGTGGAGGTGGAGGTAACT**ACG**GCCAAGATCAATCCTCCATGA

**>altFUS_Ø**

**T**GPTPPSPGRAIPSRAVSPTDSRVTVVIASPRTLQA**T**ARAAILL**T**ARARTQA**T**ELSQLPRD**T**ARLAA**T**AVARAPNRLTGSSPPTLA**T**ASSQLP
AAPREVTVAVLRAAA**T**GSPRVGATASSLA**T**VDSSKA**T**DSSKAIIPLRA**T**DSRTSTTAAVVVEVEVEVEVT**T**AKINPP

**c**

```
AltFUS      1 MGPTPPSPGRAIPSRAVSPTDSRVTVVIASPRTLQAMARAAILLMARARTQAMELSQLPR  60
AltFUS-Ø    1 TGPTPPSPGRAIPSRAVSPTDSRVTVVIASPRTLQATARAAILLTARARTQATELSQLPR  60

AltFUS     61 DMARLAAMAVARAPNRLTGSSPPTLAMASSQLPAAPREVTVAVLRAAAMGSPRVGATASS 120
AltFUS-Ø   61 DTARLAATAVARAPNRLTGSSPPTLATASSQLPAAPREVTVAVLRAAATGSPRVGATASS 120

AltFUS    121 LAMVDSSKAMDSSKAIIPLRAMDSRTSTTAAVVVEVEVEVEVTMAKINPP           170
AltFUS-Ø  121 LATVDSSKATDSSKAIIPLRATDSRTSTTAAVVVEVEVEVEVTTAKINPP           170
```

**d**

```
FUS         1 MASNDYTQQATQSYGAYPTQPGQGYSQQSSQPYGQQSYSGYSQSTDTSGYGQSSYSSYGQ  60
FUS(Ø)      1 MASNDYTQQATQSYGAYPTQPGQGYSQQSSQPYGQQSYSGYSQSTDTSGYGQSSYSSYGQ  60

FUS        61 SQNTGYGTQSTPQGYGSTGGYGSSQSSQSSYGQQSSYPGYGQQPAPSSTSGSYGSSSQSS 120
FUS(Ø)     61 SQNTGYGTQSTPQGYGSTGGYGSSQSSQSSYGQQSSYPGYGQQPAPSSTSGSYGSSSQSS 120

FUS       121 SYGQPQSGSYSQQPSYGGQQQSYGQQQSYNPPQGYGQQNQYNSSSGGGGGGGGGNYGQD 180
FUS(Ø)    121 SYGQPQSGSYSQQPSYGGQQQSYGQQQSYNPPQGYGQQNQYNSSSGGGGGGGGGNYGQD 180

FUS       181 QSSMSSGGGSGGGYGNQDQSGGGGSGGYGQQDRGGRGRGGSGGGGGGGGGYNRSSGGYE 240
FUS(Ø)    181 QSSMSSGGGSGGGYGNQDQSGGGGSGGYGQQDRGGRGRGGSGGGGGGGGGYNRSSGGYE 240

FUS       241 PRGRGGGRGGRGGMGGSDRGGFNKFGGPRDQGSRHDSEQDNSDNNTIFVQGLGENVTIES 300
FUS(Ø)    241 PRGRGGGRGGRGGMGGSDRGGFNKFGGPRDQGSRHDSEQDNSDNNTIFVQGLGENVTIES 300

FUS       301 VADYFKQIGIIKTNKKTGQPMINLYTDRETGKLKGEATVSFDDPPSAKAAIDWFDGKEFS 360
FUS(Ø)    301 VADYFKQIGIIKTNKKTGQPMINLYTDRETGKLKGEATVSFDDPPSAKAAIDWFDGKEFS 360

FUS       361 GNPIKVSFATRRADFNRGGGNGRGGRGRGGPMGRGGYGGGGSGGGGRGGFPSGGGGGGGQ 420
FUS(Ø)    361 GNPIKVSFATRRADFNRGGGNGRGGRGRGGPMGRGGYGGGGSGGGGRGGFPSGGGGGGGQ 420

FUS       421 QRAGDWKCPNPTCENMNFSWRNECNQCKAPKPDGPGGGPGGSHMGGNYGDDRRGGRGGYD 480
FUS(Ø)    421 QRAGDWKCPNPTCENMNFSWRNECNQCKAPKPDGPGGGPGGSHMGGNYGDDRRGGRGGYD 480

FUS       481 RGGYRGRGGDRGGFRGGRGGGDRGGFGPGKMDSRGEHRQDRRERPY               526
FUS(Ø)    481 RGGYRGRGGDRGGFRGGRGGGDRGGFGPGKMDSRGEHRQDRRERPY               526
```

928 **Extended Data Figure 3**

929 **a**, Object image from MicroP processing of images of mock and altFUS transfected HeLa cells.
930 Tubules are coloured in purple, globules are coloured in green. **b**, Graphical representation of
931 bicistronic constructs FUS and FUS-R495x (mutation in red), and their monocistronic equivalent
932 $FUS^{(\emptyset)}$ and $FUS^{(\emptyset)}$-R495x. AltFUS CDS is highlighted in green when present, FUS CDS is highlighted
933 in blue. **c**, V5-FUS, V5-FUS-R495x and altFUS-FLAG expression from bicistronic or monocistronic
934 constructs in HEK293 cells (representative image from n=3). **d**, Representative traces of TMRE
935 fluorescence measured by flow cytometry in mock cells and cells overexpressing the bicistronic
936 constructs FUS or FUS-R495x (in red) in the top panels, and the monocistronic constructs, $FUS^{(\emptyset)}$
937 or $FUS^{(\emptyset)}$-R495x (in blue) in the bottom panels (n=3, minimum of 50 000 live cells per independent
938 replicates).

939

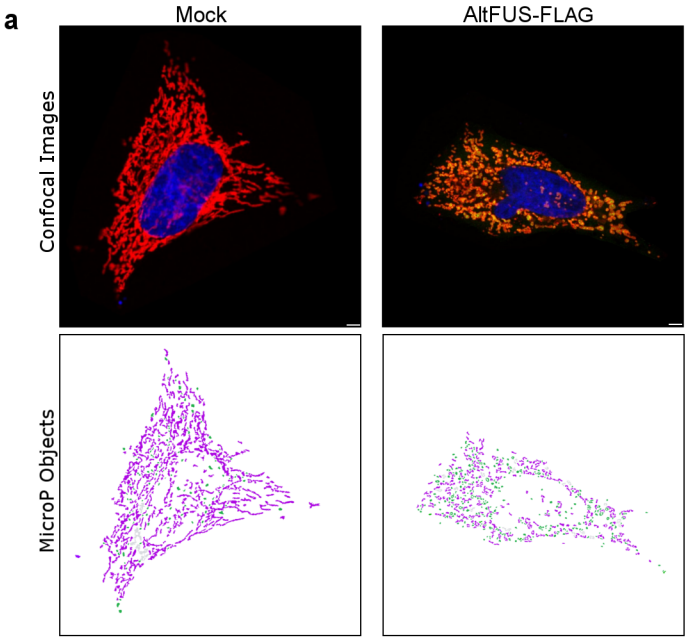
a
Mock
AltFUS-FLAG
Confocal Images
MicroP Objects

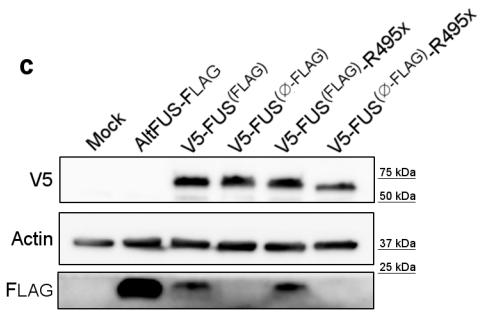
c
Mock
AltFUS-FLAG
V5-FUS(FLAG)
V5-FUS(∅-FLAG)
V5-FUS(FLAG)-R495x
V5-FUS(∅-FLAG)-R495x
V5
Actin
FLAG
75 kDa
50 kDa
37 kDa
25 kDa

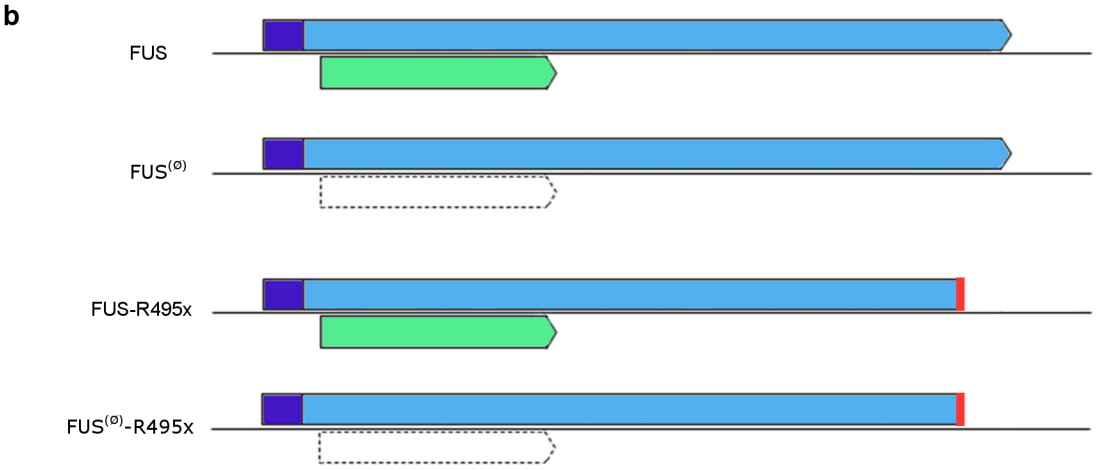
b
FUS
FUS(∅)
FUS-R495x
FUS(∅)-R495x

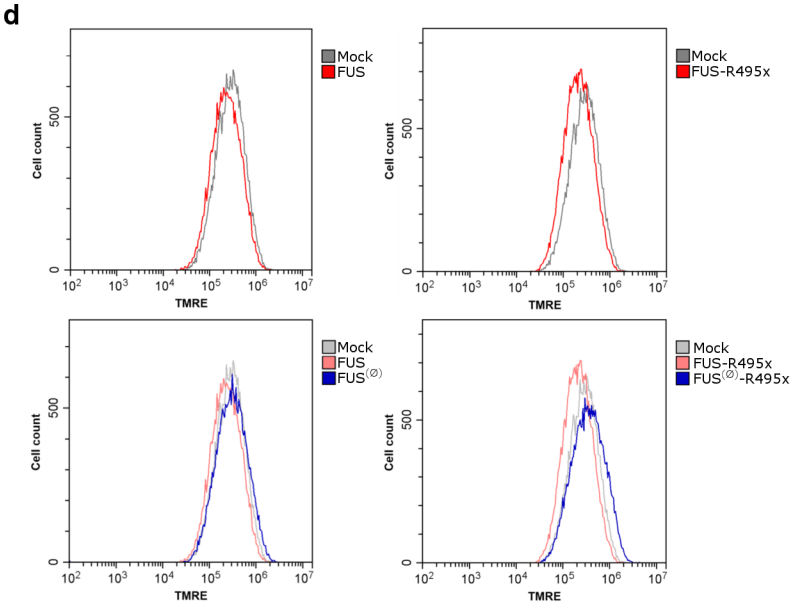
d
Mock
FUS
FUS-R495x
FUS(∅)
FUS(∅)-R495x
Cell count
TMRE

940 **Extended Data Figure 4**

941 **a**, Graphical representation of the mCherry-GFP-LC3 construct to study the autophagic flux. **b**,
942 Images by confocal microscopy of mCherry-GFP-LC3 and altFUS (FLAG, in blue) signal in HeLa cells
943 across biological conditions: untreated mock, bafilomycin treated mock, altFUS, FUS, FUS$^{(Ø\text{-}FLAG)}$,
944 FUS-R495x and FUS$^{(Ø\text{-}FLAG)}$-R495x (representative images of n=3). The white scale bar corresponds
945 to 10µm and the zoomed in region (right panel) is delimited as a white box. **c**, LC3-II expression
946 from untreated (-) or bafilomycin treated (+) cells transfected with mock, altFUS, FUS, FUS$^{(Ø)}$, FUS-
947 R495x, FUS$^{(Ø)}$-R495x, or co-transfected with FUS$^{(Ø)}$-R495x and altFUS. **d-f**, Images by confocal
948 microscopy of FLAG (white), GFP (green) and TDP-43 (red) signals in HeLa cells transfected with
949 the bicistronic constructs (**d**), monocistronic constructs (**e**) or co-transfected with altFUS-FLAG and
950 the monocistronic constructs (**f**) of 6 ALS-associated mutants: FUS-G156E, FUS-K510E, FUS-
951 Q519x, FUS-Q519I-fs527x, FUS-R521C, and FUS-P525L (representative images from n=3). The
952 white scale bar corresponds to 10µm.

953

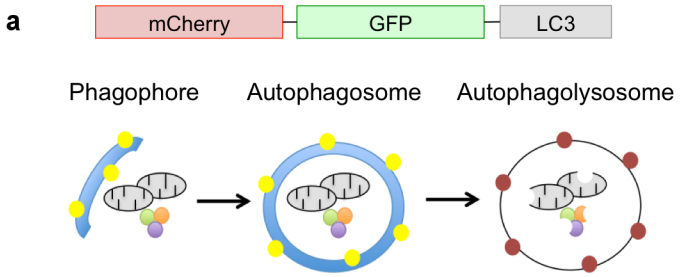
a
mCherry
GFP
LC3
Phagophore
Autophagosome
Autophagolysosome

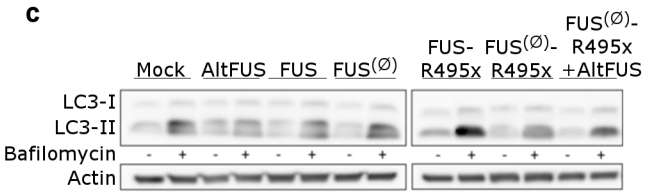
c
Mock
AltFUS
FUS
FUS(Ø)
FUS-R495x
FUS(Ø)-R495x
FUS(Ø)-R495x +AltFUS
LC3-I
LC3-II
Bafilomycin
Actin

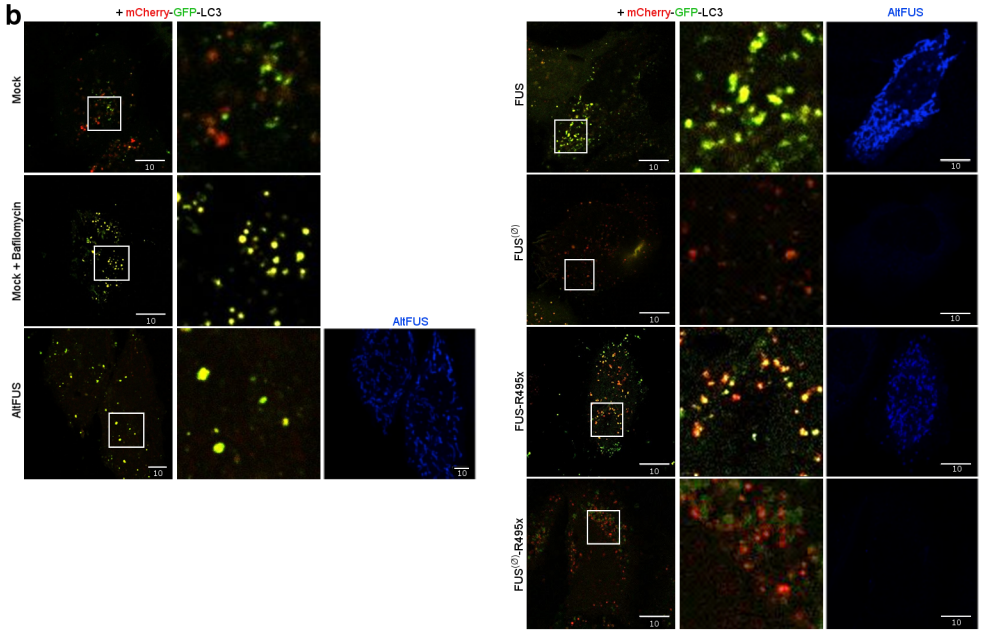
b
+ mCherry-GFP-LC3
AltFUS
Mock
Mock + Bafilomycin
AltFUS
FUS
FUS(Ø)
FUS-R495x
FUS(Ø)-R495x

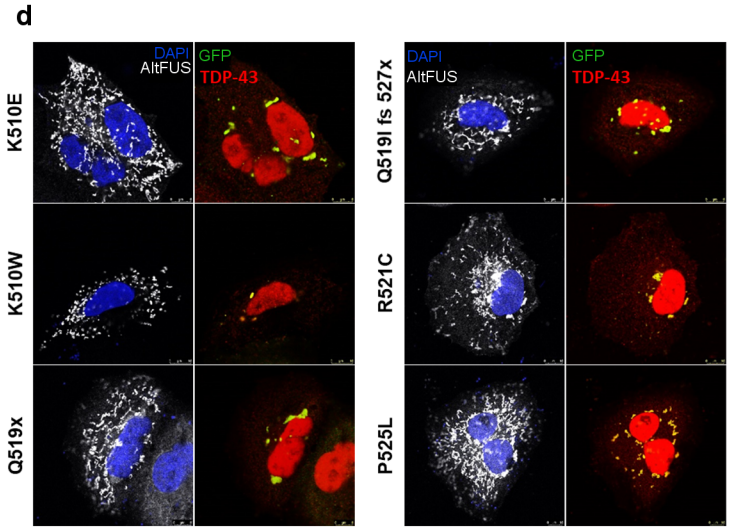
d
DAPI
AltFUS
GFP
TDP-43
K510E
K510W
Q519x
Q519I fs 527x
R521C
P525L

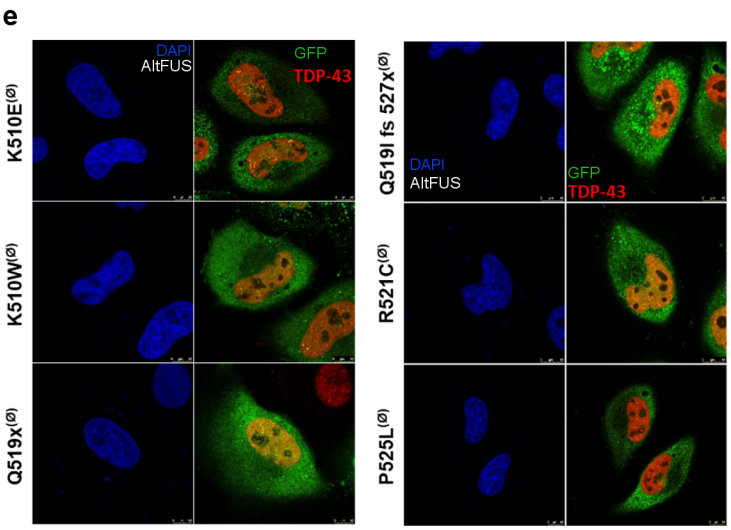
e
DAPI
AltFUS
GFP
TDP-43
K510E(Ø)
K510W(Ø)
Q519x(Ø)
Q519I fs 527x(Ø)
R521C(Ø)
P525L(Ø)

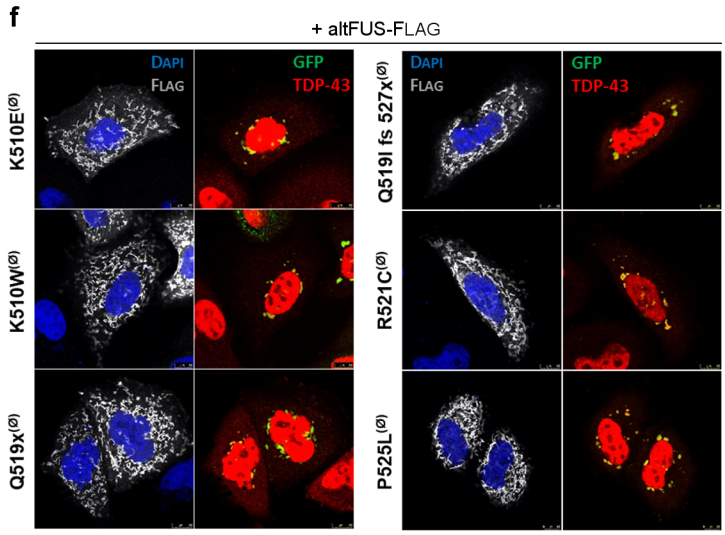
f
+ altFUS-FLAG
DAPI
FLAG
GFP
TDP-43
K510E(Ø)
K510W(Ø)
Q519x(Ø)
Q519I fs 527x(Ø)
R521C(Ø)
P525L(Ø)

954 **Extended Data Figure 5**

955 **a**, Images by confocal microscopy of FLAG (white), GFP (green) and TIA-1 (red) signals in HeLa cells
956 transfected with the bicistronic GFP-FUS$^{(FLAG)}$-R495x or the monocistronic GFP-FUS$^{(Ø\text{-}FLAG)}$-R495x
957 constructs, or co-transfected with the monocistronic GFP-FUS$^{(Ø\text{-}FLAG)}$-R495x and altFUS-FLAG
958 constructs (representative images from n=3). The white scale bar corresponds to 10µm. **b-d**,
959 Images by confocal microscopy of FLAG (white), GFP (green) and TIA-1 (red) signals in HeLa cells
960 transfected with the bicistronic constructs (**b**), monocistronic constructs (**c**) or co-transfected with
961 altFUS-FLAG and the monocistronic constructs (**d**) of 6 ALS-associated mutants: FUS-G156E, FUS-
962 K510E, FUS-Q519x, FUS-Q519I-fs527x, FUS-R521C, and FUS-P525L (representative images from
963 n=3). The white scale bar corresponds to 10µm.

964

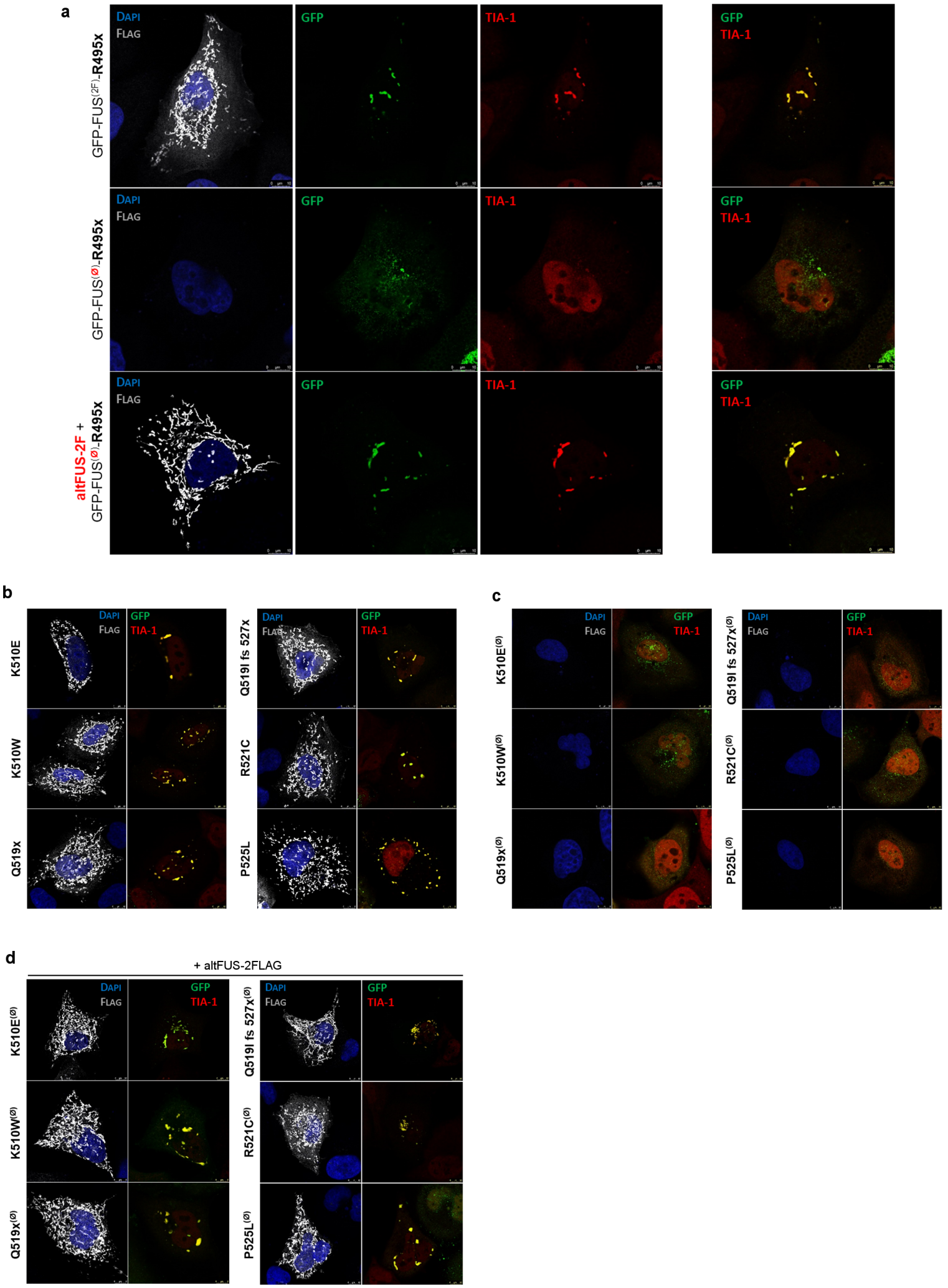
a
GFP-FUS(2F)-R495x
GFP-FUS(Ø)-R495x
altFUS-2F +
GFP-FUS(Ø)-R495x
DAPI
FLAG
GFP
TIA-1
b
K510E
K510W
Q519x
Q519I fs 527x
R521C
P525L
c
K510E(Ø)
K510W(Ø)
Q519x(Ø)
Q519I fs 527x(Ø)
R521C(Ø)
P525L(Ø)
d
+ altFUS-2FLAG